Biology of Reproduction, 2023, **108(3)**, 447–464
https://doi.org/10.1093/biolre/ioad001
Advance access publication date 6 January 2023
Research Article

Actin-related protein ACTL7B ablation leads to OAT with multiple morphological abnormalities of the flagellum and male infertility in mice†

Tracy M. Clement[1,†,*], Christopher B. Geyer[2,3], William D. Willis[4], Eugenia H. Goulding[4], Srijana Upadhyay[1] and Edward M. Eddy[4,†]

[1]Department of Physiology and Pharmacology, College of Veterinary Medicine and Biomedical Sciences, Texas A&M University, College Station, USA
[2]Department of Anatomy and Cell Biology, Brody School of Medicine, and East Carolina Diabetes and Obesity Institute East Carolina University, Greenville, USA
[3]East Carolina Diabetes and Obesity Institute East Carolina University, Greenville, USA
[4]Gamete Biology Group, Reproductive and Developmental Biology Laboratory, National Institute of Environmental Health Sciences, National Institutes of Health, Research Triangle Park, Durham, USA

*__Correspondence__: Texas A&M University, VTPP 4466, College Station, TX 77843-4466, USA. E-mail: tclement@tamu.edu

†__Grant Support__: This research was supported by the Eunice Kennedy Shriver National Institute of Child Health & Human Development of the National Institutes of Health (K99/R00HD081204 awarded to TMC), by the Intramural Research Program of the NIH; National Institute of Environmental Health Sciences (ZIA ES070076 awarded to EME); and by start-up funds from Texas A&M University (to TMC). The content is solely the responsibility of the authors and does not necessarily represent the official views of the National Institutes of Health.

Abstract

The formation of fertilisation-competent sperm requires spermatid morphogenesis (spermiogenesis), a poorly understood program that involves complex coordinated restructuring and specialised cytoskeletal structures. A major class of cytoskeletal regulators are the actin-related proteins (ARPs), which include conventional actin variants, and related proteins that play essential roles in complexes regulating actin dynamics, intracellular transport, and chromatin remodeling. Multiple testis-specific ARPs are well conserved among mammals, but their functional roles are unknown. One of these is actin-like 7b (*Actl7b*) that encodes an orphan ARP highly similar to the ubiquitously expressed beta actin (ACTB). Here we report ACTL7B is expressed in human and mouse spermatids through the elongation phase of spermatid development. In mice, ACTL7B specifically localises to the developing acrosome, within the nucleus of early spermatids, and to the flagellum connecting region. Based on this localisation pattern and high level of sequence conservation in mice, humans, and other mammals, we examined the requirement for ACTL7B in spermiogenesis by generating and characterising the reproductive phenotype of male *Actl7b* KO mice. KO mice were infertile, with severe and variable oligoteratozoospermia (OAT) and multiple morphological abnormalities of the flagellum (MMAF) and sperm head. These defects phenocopy human OAT and MMAF, which are leading causes of idiopathic male infertility. In conclusion, this work identifies ACTL7B as a key regulator of spermiogenesis that is required for male fertility.

Received: July 17, 2020. **Revised:** October 11, 2022. **Accepted:** December 30, 2022

Graphical Abstract

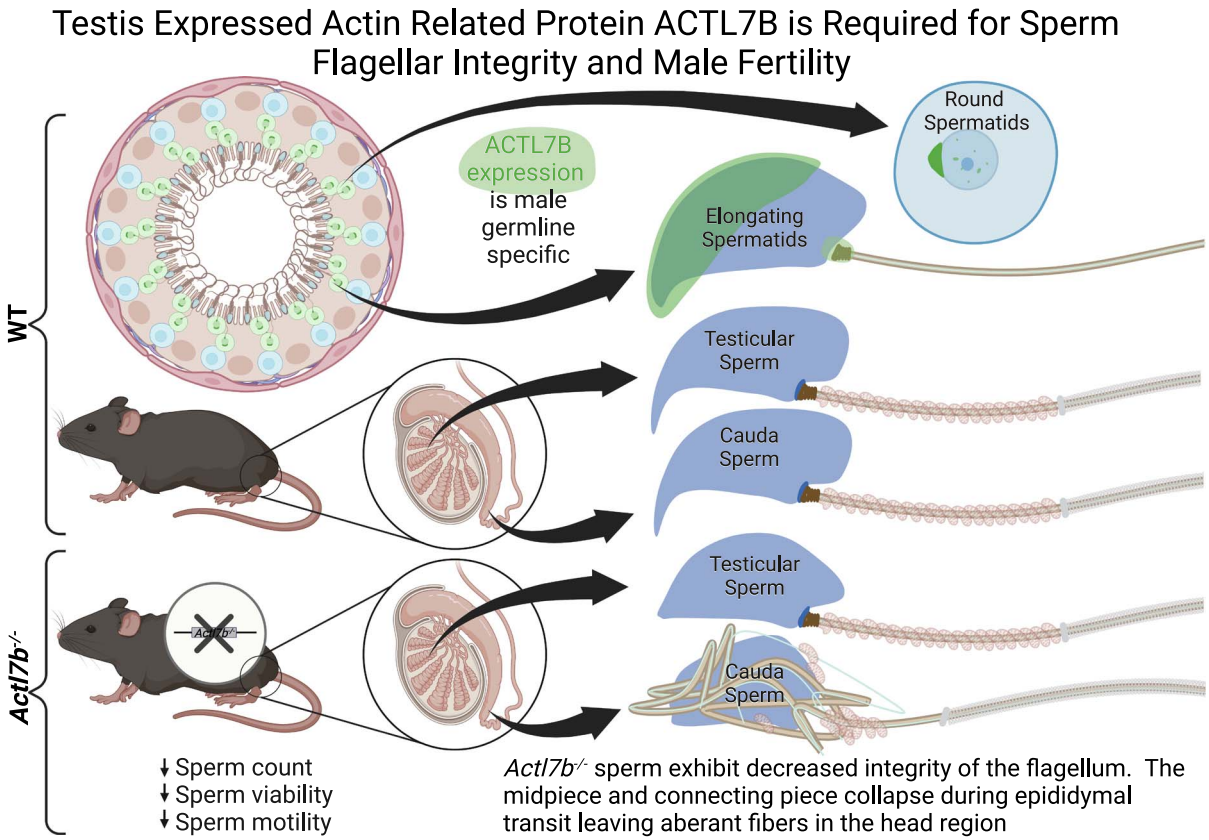

Introduction

Fertility and infertility are both highly personal and significant societal issues. It is estimated that half of all pregnancies are unintended [1], and yet there remains a dearth of male contraceptive options. Conversely, it is also estimated that infertility affects between 10 and 15% of couples, with half of the cases traced to contributing factors from the male partner [2]. Half of these cases of male infertility are idiopathic, but are often associated with high incidence of morphological abnormalities of the sperm [3]. Defining the molecular mechanisms responsible for male fertility and identifying potential contraceptive targets requires continued progress toward understanding factors critical for spermatogenesis.

The production of sperm during spermatogenesis occurs in a highly ordered manner. It begins with spermatogonial stem cells, whose progeny proliferate and ultimately differentiate to give rise to meiotic spermatocytes. Spermatocytes complete meiosis to produce haploid round spermatids, which then undergo complex morphogenic restructuring during the process of spermiogenesis. During spermiogenesis, spermatids undergo dramatic cellular and nuclear reshaping, their chromatin is condensed, excess cytoplasm is eliminated, and they develop unique organelles and a flagellum (reviewed in [4]). Although the structural components and morphological changes in this complex process have been described in detail, relatively little is known about the intrinsic spermatid specific molecular mechanisms responsible for reshaping spermatids into functional sperm. This is due in part to the large number of genes uniquely expressed in the mammalian testis, only a fraction of which have been investigated for a functional requirement in male fertility [4–18].

The extensive morphological changes that spermatids undergo during spermiogenesis are accompanied by relocalisation of actins [19–26] and formation of transient actin-rich structures such as the manchette and acroplaxome. Thus, it is apparent that dramatic and dynamic changes in the cytoskeleton play essential structural and functional roles during spermiogenesis. In somatic cells, dynamic cellular actin pools are regulated by numerous actin-binding proteins (ABPs) and actin regulatory proteins. These proteins act together to meet the cellular demand for cytoskeletal rearrangement by directing transitions between filamentous (F)-actin structures and monomeric or globular (G)-actin pools [27]. Transitions between G- and F-actin direct cell shapes are responsible for cellular polarity, motility, intracellular transport, and organelle localisaation. Disruption of these finely tuned processes can lead to a variety of disease states including muscle myopathies, compromised immunity, neurodegeneration, and cancer metastasis [27–29]. Moreover, monomeric actin also associates with multimeric protein complexes mediating intracellular transport and chromatin remodeling in somatic cells [30, 31]. Actin-related protein (ARP) family members have a conserved actin fold domain and serve functionally diverse but evolutionarily conserved cellular functions [32]. ARP functions include essential roles building, nucleating, and branching conventional actin filaments, as well as facilitating dynein cargo transport, and altering chromatin structure [28, 29, 31]. This diversity of critical somatic cell functions indicates the broad functionality

of these essential somatic ARPs. However, the role of these ARPs during spermiogenesis has not been established.

Actin-like 7b (*Actl7b*) is a functionally uncharacterised intronless gene encoding an ARP sharing ~40% sequence homology to conventional filament-forming actins and lacking genomic insertions or deletions that define conserved genes encoding other ARP family members across species [32–34]. ACTL7B contains the conserved protein kinase C and cAMP/cGMP phosphorylation sites of ARPs and a unique N-terminal sequence [35]. The testis-specific *Actl7b* is expressed in mouse testes as early as 23 days post-partum (dpp), which is roughly coincident with the appearance of round spermatids [34]. Furthermore, *Actl7b* is highly conserved among mammals with mouse and human *Actl7b* being 83% identical at the nucleotide level and 91% similar at the amino acid level. Interestingly, SNPs have been identified in *ACTL7B* in sterile human men suggesting a causative role in human male factor infertility [36]. Together, the high level of evolutionary conservation and spermatid-specific expression led us to posit an essential role for ACTL7B in the formation of fertilisation-competent sperm. In this study, we tested this hypothesis by generating and characterising *Actl7b* knock-out (KO) mice. KO mice have sperm with malformed flagella revealing an essential functional role of ACTL7B in spermatid morphogenesis, which is essential for the formation of fertilisation-competent sperm and thus male fertility.

Materials and methods

Generation of Actl7b-null mice

Mouse embryonic stem cells (ESCs) with the coding sequence of the *Actl7b* gene replaced with an LacZ reporter gene were acquired from the KOMP repository (ID# VG10808). The ESCs were derived from C57BL/6NTac (black coat color) mice and were injected into 97 C57BL/6 J-*Tyr*$^{c\text{-}2J}$ (white coat color) mouse blastocysts transferred into nine pseudopregnant recipient CD1 females. This resulted in 18 live pups, of which 9 were high-percentage black coat-color male chimeras. Five male chimeras exhibited germ-line transmission when backcrossed with C57BL/6 N females to produce *Actl7b*$^{+/-}$ (Het) mice. Male and female Het breeding produced *Actl7b*$^{-/-}$ (KO), as well as the Het and WT littermate controls. Genotypes were determined by standard PCR using the following primers: KO allele = forward 5'-TTCGGCTATGACTGGGCACAACAG and reverse 5′-CTTCCTCTCTGGAAACGCTG; WT allele = forward 5'-GCTGGAGACAACTTCAAGGAG, and reverse 5'-GGGCA GAGGAGACTCAAC. Mice were housed on a 12-h light/dark cycle with *ad libitum* access to food and water. All protocols were in accordance with the Guide for Care and Use of Laboratory Animals by the National Institute of Health, and studies were approved by the NIEHS or Texas A&M Institutional Animal Care and Use Committees (IACUC #2018-0104).

Data availability

The data underlying this article are available in the article and in its online supplementary material.

Human testicular tissue

Human testicular tissue was obtained from an 18-year-old, apparently healthy black male who received an orchiectomy at Vidant Medical Center (Greenville, NC) following acute scrotal trauma. Tissues were fixed and prepared for IHC as described [37]. The protocol for the collection and utilisation of human testicular tissue was approved by the East Carolina University Institutional Review Board (UM-CIRB# 10_0627).

LacZ staining

Tissues were collected and fixed in 4% paraformaldehyde for 1 hour at room temperature. They were then washed and stained by incubation in LacZ buffer as described [38].

Fertility assessment and tissue preparation

KO males (2–4 months old) and WT littermate controls were individually housed with two WT C57BL/6 N females for 2 months. Normal mating behavior was confirmed by the presence of copulatory plugs. After 1 month, females were replaced with two new WT females for an additional month. The parturition dates, litter sizes, and pup sex ratios were recorded. Following completion of the breeding studies, males (4–6 months old) were euthanised and body, spleen, testes, epididymal, and seminal vesicle weights were recorded. A testis with attached epididymis was fixed in Bouin's solution at 4°C overnight, dehydrated in ethanol, and embedded in paraffin. The contralateral testis was snap-frozen in liquid nitrogen for protein isolation and the contralateral cauda epididymis was rinsed in 1X PBS and placed into either 1X PBS (Ca^{2+}/Mg^{2+} free) or EmbryoMax M2 media (EMD Millipore, Billercia, MA), which was pre-equilibrated to 37°C, and several small cuts were made with iridectomy scissors to allow for sperm to swim out into the media over a 15-min incubation at 37°C. No age-dependent differences were observed, and data are representative of all males of a specific genotype.

Sperm analyses

Sperm were counted using a Neubauer chamber with standard methods. To calculate the percent "motile" sperm, all sperm in randomly selected fields of view were counted until at least 300 sperm per sample were tallied as motile or immotile defined as the presence or absence of even minimal flagellar motion, respectively. Videos of sperm motility in M2 media were recorded on an inverted Olympus microscope with a Retiga camera (QImaging, Surrey, BC Canada) at 8 frames/second. The localisation of mitochondria in spermatozoa was determined by incubating 10-μl MitoTracker deep red FM (Life Technologies, Grand Island, NY) with a 90-μl aliquot of sperm at 37°C for 45 minutes. Sperm were washed in 1X PBS, allowed to settle onto chilled poly-L-lysine coated glass slides and fixed with 4% (w/v) paraformaldehyde. For chromomycin A3 (CMA3) chromatin compaction assays, settled sperm were permeabilised with 0.5% NP40 in PBS for 2 minutes, then stained with a 0.25 mg/mL CMA3 (Millipore-Sigma) solution in 10-mM $MgCl_2$, 164-mM Na_2HPO_4, and 17-mM citric acid, pH 7.0) for 20 minutes. For F-actin staining, sperm settled on poly-L-lysine slides were incubated with a 1:400 dilution of Phalloidin-AlexaFluor-488 (Invitrogen, Waltham MA) for 1 hour. DNA counterstaining is Hoechst 33342 or DAPI (Life Technologies, Waltham MA). Sperm slides were mounted in ProLong Gold antifade reagent (Life Technologies, Waltham MA). A minimum

of 200 sperm were counted for each of $n = 3$ mice per genotype.

Ultrastructure analysis

Sperm were isolated for scanning electron microscopy (SEM) as described above, collected on poly-L-lysine coated glass coverslips (BD BioCoat, Bedford, MA), and fixed overnight at 4°C in 0.2% picric acid, 2.5% glutaraldehyde, and 2% paraformaldehyde in 0.1-M sodium phosphate buffer at pH 7.4. Testes and epididymides were fixed for transmission electron microscopy (TEM) in the same fixative overnight. All samples were then processed as described previously [39, 40]. Samples were examined with a Zeiss TEM 910 with a digital interface and Gatan SC1000 camera or a Zeiss Supra 25 Field Emission SEM, located in the Microscopy Services Laboratory at the University of North Carolina School of Medicine.

Histology, immunohistochemistry (IHC)and immunofluorescence (IF)

For histological analyses, 5-μm paraffin sections were stained with hematoxylin and/or eosin using standard methods. IHC was performed as previously described [41]. Briefly, goat anti-ACTL7B primary antibodies (Novus Biologicals (Imgenex, Littleton, CO) were diluted 1:400, secondary antibody was fluorophore labeled donkey anti-goat antibody (Vector Laboratories, Burlingame, CA) used at a 1:400 dilution, followed by incubation with ready-to-use horseradish peroxidase-streptavidin and ImmPACT DAB (both from Vector Labs, Newark CA), and counterstained with hematoxylin. Sperm for IF were fixed and stained as previously described [42], and individual spermatids were prepared and stained as previously described [40]. Primary antibodies used were as follows: goat anti-ACTL7B (Novus Biologicals (Imgenex, Littleton, CO, 1:300), rabbit anti-ODF2 (kind gift of Dr. Frans A. van der Hoorn, 1:2000 [39, 43], mouse anti-α-Tubulin (Sigma Aldrich, St Louis, MO, 1:600). To generate anti-AKAP3, the full-length mouse *Akap3* coding sequence was cloned into a pET-28a expression vector (EMD Millipore, Darmstadt Germany), transformed into BL-21(DE) bacteria, expression induced using IPTG, and the resulting protein was purified using the fused His-Tag. The purified protein was injected into two NZW rabbits to produce antibodies (Covance, Princeton, NJ), the serum was affinity purified over a PROSEP-A column (EMD Millipore, Darmstadt Germany), and the antibody was used at a 1:100 dilution. Secondary antibodies used for IF were donkey anti-rabbit-AlexaFluor-488, anti-mouse-AlexaFluor-488 and 546, and anti-goat-AlexaFluor-488 (Life Technologies, Waltham MA). Slides were mounted in ProLong Gold antifade reagent with DAPI (Life Technologies, Waltham MA). Images were obtained using a Zeiss 710 inverted multiphoton laser-scanning microscope with 405, 488, and 561 lasers and a Zeiss Plan-Apochromat 63X (1.4 na) oil immersion objective or Leica DMi8 modular inverted microscope for brightfield, phase contrast, DIC, and fluorescence imaging, with Sola light engine, DMC2900 CMOS color camera, and DFC9000 GT sCMOS monochrome camera.Images were scanned and analysed using Zenn 2010 software (Zeiss, Oberkochen, Germany) or LAS X software (Leica Microsystems, Wetzalar, Germany) for image capture and processing.

Western blotting

Protein lysates from testis were prepared by lysing one adult mouse testis in 1-ml cold RIPA buffer in a Dounce homogeniser. Gel electrophoresis of testis lysates and transfer blotting were performed according to standard protocols using BioRad 4–20% mini-protein TGX gels and 1X BioRad Tris/Glycine/SDS running buffer, tris/glycine transfer buffer, and PVDF membranes (BioRad, Hercules CA). Blots were then blocked overnight with 0.1% Tween20 and 5% dry milk in PBS. Primary antibodies were incubated in PBS-T 1:1500 for 2 hours, followed by HRP conjugated secondary antibodies in PBS-T at 1:20 000 for1 hour. Pierce ECL western blotting substrate was used to detect the HRP-conjugated secondary antibodies. Primary antibodies to ACTL7B were Novus Biological goat anti-ACTL7B recognising a C-terminal aa278-290 (DELHVDYELPDGK) (Novus Biologicals (Imgenex, Littleton, CO), or custom-made rabbit antibodies to N-terminal peptides. To generate the N-terminal anti-ACTL7B antibodies, immunising peptides of >85% purity were synthesised and conjugated to KLH with the following peptide sequences; Ac-KNSPSPKPMGTAQGDPGEC-KLH corresponding to nucleotides 4–21 of the mRNA, or Ac-RDTGSTQLKTKPKKIRKIKC-KLH corresponding to nucleotides 34–52. The immunising peptides were injected into rabbits by Pocono Rabbit Farm & Laboratory (PRF&L, Canadensis PA) following their 91-day protocol. Bleeds were screened for appropriate response by western blotting and IF and the best bleed was affinity purified with the immunising peptide conjugated to a sulfolink column (PRF&L, Canadensis, PA).

Cell death assays

For cell death assays on tissue sections, 5-μm paraffin sections of Bouins fixed tissue were assayed with the In Situ Cell Death Detection Kit, POD (Roche, Mannheim, Germany) following the manufacture's recommendations, and counter-stained with hematoxylin. Sperm TUNEL assays were carried out using sperm from cauda epididymides collected in Human Tubal Fluid (HTF) medium (Millipore Sigma, Darmstadt, Germany), fixed with 4% paraformaldehyde, and washed and re-suspended in 1X PBS. Sperm suspensions were allowed to settle for 2 hours at RT on polylysine coated slides and permeabilised using 0.5% NP40 for 2 minutes. The Click-iT Plus TUNEL Assay kit (Invitrogen, Waltham MA) was used following the manufacture's protocol. Sperm were counter stained with Hoechst 33342 dye (Scientific, Waltham, MA) and mounted in Prolong Gold antifade reagent (P36930, Thermo Fisher Scientific, Waltham, MA). Images were acquired using an LEICA DMi8 imaging system. A minimum of 200 sperm were counted for each of $n = 3$ mice per genotype.

Statistical analyses

A minimum of three biological replicates was included in all assessments. Mean values ± SEM were calculated for each quantitative parameter, and error bars in all figures represent SEMs. GraphPad Prism 4 was used for statistical analysis (GraphPad Software, San Diego, CA). Two-tailed Student's *t*-tests were performed to assess statistical differences between KO and WT organ weights and sperm counts. Differences were considered significant at $P < 0.05$.

Results

ACTL7B is restricted to spermatids with developmental-stage-dependent subcellular localisation

To investigate the role of ACTL7B in the testis, we first determined its precise spaciotemporal expression. Previous studies showed that *Actl7b* transcripts were first detectable in the mouse testis at 23 dpp [34, 35], suggesting expression in early stage round spermatids. We first determined the cell specificity of its protein expression pattern in the testis during spermatogenesis (Fig. 1). The 16 steps of spermatid development in the mouse are defined by their consistent associations with specific cohorts of germ cells during the 12 stages of the seminiferous epithelial cycle [44]. Using IHC, we detected ACTL7B in the cytoplasm and nuclei of round and elongating spermatids in Stages I-XII (brown staining in Fig. 1A–F), but not in other testicular cells including the subsequent condensing spermatids. We also detected ACTL7B in round and elongating spermatids in the human testis (Fig. 1G, brown staining), suggesting a conserved expression pattern and role in humans.

To precisely define the intracellular localisation of ACTL7B, spermatids isolated from segments of seminiferous tubules were used for immunostaining. ACTL7B was localised primarily to the acrosomal region in acrosomal capping phase round spermatids and during spermatid elongation. This was seen as a cap-like structure over nuclei in steps 5–8 and 9–11, respectively (Fig. 1H–L). Immunolocalisation of ACTL7B was also observed in a speckled pattern in the nuclei of steps 3–5 round spermatids (Fig. 1H, step 5 shown). Later in spermatid morphogenesis, ACTL7B was also localised in the connecting piece between the head and flagella of elongating spermatids (Fig. 1K–L, arrows) before becoming undetectable in steps 13–16 condensing spermatids (Fig. 1H–J). These findings are consistent with previous reports that ACTL7B was undetectable in sperm [34, 35].

ACTL7B is required for male fertility

Little is known about the cell-autonomous roles of cytoskeletal dynamics and testis-specific ARPs during the morphogenic changes that reshape spermatids into fertilisation-competent sperm. To define the specific role for ACTL7B in spermatogenesis, we generated KO mice from mouse ESCs in which the coding sequence of the intronless *Actl7b* gene was replaced by a β-galactosidase reporter gene (Fig. 2A and Supplementary Fig. S1). We performed β-gal staining on testes and epididymides (Fig. 2B and Supplementary Fig. S1) to confirm LacZ replacement of *Actl7b* in the testis. β-gal was detectable in epididymides from both HET and $Actl7b^{+/+}$ (WT) mice; this was not surprising, as the epididymis has endogenous β-galactosidase activity [45, 46]. However, within the testis, seminiferous epithelium β-gal was solely detectable in Het mice, revealing expression originating from the LacZ replacement of the *Actl7b* coding region. Other organs did not demonstrate specific Lac-Z staining with the exception of brain (Supplementary Fig. S1), which exhibited a low level of staining only after overnight incubation (12–16 hours more than testis), suggesting a very low level of expression under the *Actl7b* promoter in the brain of this mouse model.

Male and female Het mice were bred to generate $Actl7b^{-/-}$ (KO) mice. Crosses between Het mice produced normal litter sizes with expected Mendelian offspring ratios, indicating the

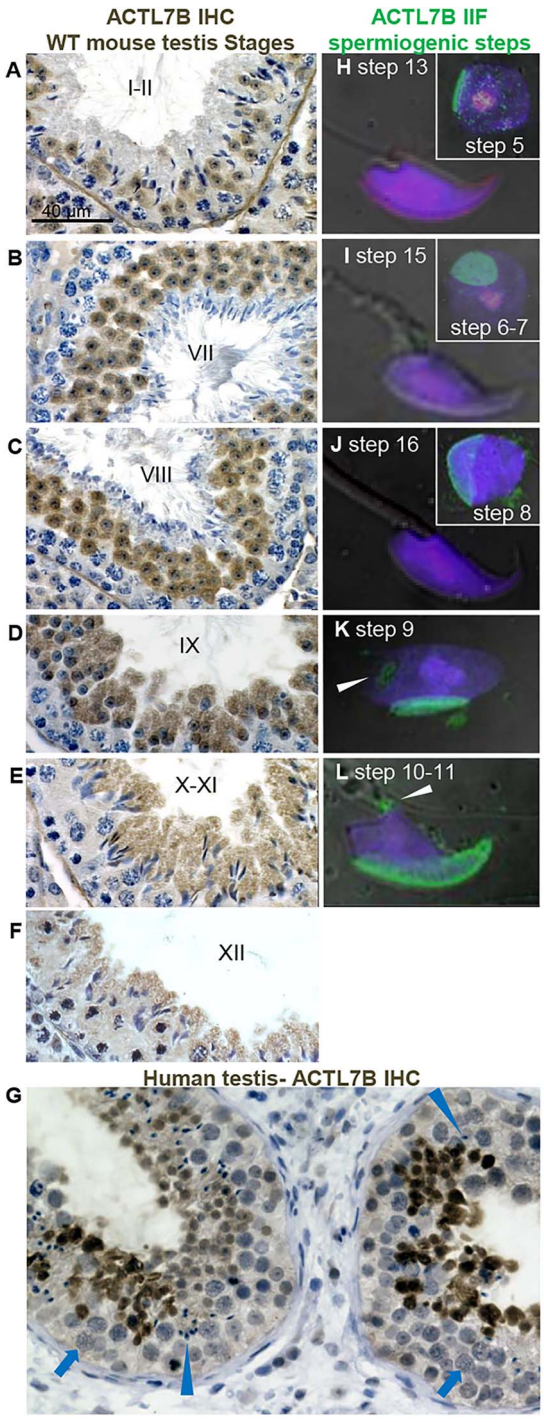

Figure 1. ACTL7B is expressed in mouse and human spermatids. (A–F) ACTL7B immunohistochemistry (brown staining) on mouse testis sections counterstained with hematoxylin (blue). Scale bar in (A) is 40 μm and is representative for (A)–(F). Roman numerals indicate the Stage of the seminiferous epithelium for each tubule. ACTL7B is detected in round and elongating spermatids in each Stage. (H–L) ACTL7B IIF (green) on mechanically separated spermatids, and nuclei are stained with DAPI (blue). The specific step of the development of each spermatid is indicated; where two steps of spermatid development are present in the same tubule Stage, the earlier round spermatid step is shown in the inset box. White arrows indicate the presence of ACTL7B at the head-tail connecting piece in step 9 and 11 spermatids. (G) IHC localisation of ACTL7B in the human testis, counterstained with hematoxylin (blue). ACTL7B is detectable in round and elongating spermatids (brown staining), but not spermatocytes (arrows) or condensed spermatids (arrowheads).

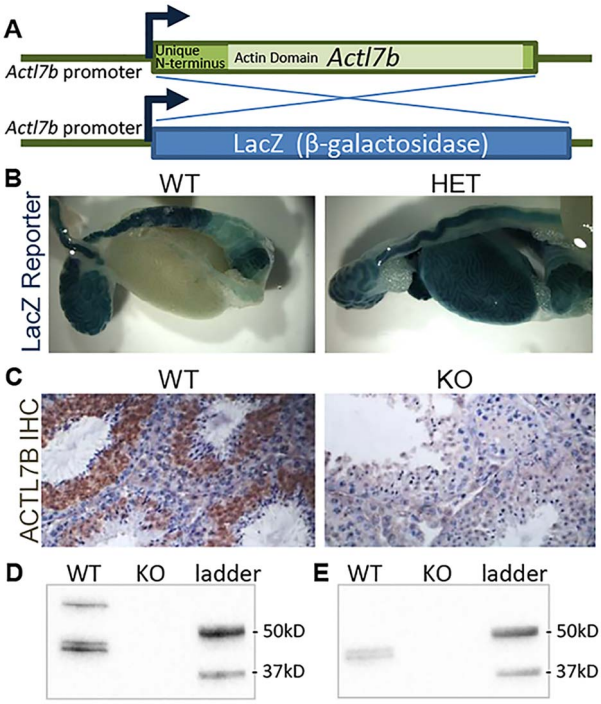

Figure 2. *Actl7b* KO in mice was confirmed. (A) Targeted mutation of *Actl7b* resulted in replacement of the single exon coding region with a sequence coding expression of β-galactosidase under the direction of the endogenous *Actl7b* promoter. (B) LacZ staining (blue) in testis of WT and *Actl7b*$^{+/-}$ (HET) mouse tissues in which β-galactosidase is expressed under control of the *Actl7b* promoter. (C) Confirmation of the absence of ACTL7B in KO mice by immunohistochemical staining of ACTL7B (brown staining) in WT and KO testes. (D and E) Western blots detecting expression of ACTL7B in WT and KO testis tissue lysates using an antibody to an ACTL7B C-terminal peptide (D), or N-terminal peptide (E) to confirm the absence of ACTL7B in the KO.

lack of a haploinsufficiency fertility defect in this genetic background. To confirm the deletion of *Actl7b*, IHC was performed on sections from adult WT and KO testes; in contrast to WT, ACTL7B was undetectable in KO testes (Fig. 2C). Further, western blotting using two separate antibodies for ACTL7B showed bands of expected sizes in the WT testis lysates were absent in *Actl7b* KO testis lysates (Fig. 2D–E).

KO male and female mice matured to adulthood without apparent health defects and exhibited normal mating behaviors. The requirement for ACTL7B in male fertility was assessed by entering WT and KO littermates into a 2-month breeding trial with two WT females per male. Each of the 10 WT males sired multiple litters of expected sizes averaging 6.8 ± 0.37 pups per litter. In contrast, none of the 10 KO males sired offspring (Fig. 3A). Testis and epididymis weights of KO mice from this trial were reduced 20% compared to WT littermates, whereas whole body and other organ weights were not significantly different (Fig. 3B–C). Paired seminal vesicle weights did not differ between WT and KO mice, suggesting endocrine signaling was not disrupted in KO mice. Cauda epididymal sperm counts from KO mice were reduced ~10-fold compared with WT mice (Fig. 3D), and sperm from KO mice lacked apparent forward progressive motility. Less than 1% of KO sperm exhibited any detectable flagellar movement (Supplementary movies 1 and 2). In addition, it was noted that flagellar midpiece segments were diminished. Quantitative analyses revealed a significant percentage of KO sperm were lacking midpieces, or exhibited wrapped flagella that precluded assessment of the midpiece length (Fig. 3E–F). In KO mice, ~30% of sperm exhibited flagella wrapped around the head, and 25% of sperm lacked the midpiece, contrasting with WT sperm in which >99% of sperm exhibited normal midpieces (Fig. 3G) and representative images are shown (Fig. 3F). The average length of the midpiece in KO sperm was reduced as well (8.7 μm in KO versus 20.2 μm in WT sperm, Fig. 3G).

Severe and variable teratozoospermia occurs in KO mice

Cauda epididymal sperm from WT and KO mice were examined by SEM to examine the ultrastructure of KO sperm (Fig. 4). Compared with WT sperm (Fig. 4A and C), KO sperm displayed severe teratozoospermia with irregular and variable structural defects in the heads and flagella (Fig. 4B, D–F). The regions of the flagellum from proximal to distal are the connecting piece, midpiece, annulus, principal piece, and end piece that are all observable in the WT sperm (Fig. 4A and G'). SEM confirmed the midpiece was absent in many KO sperm and thin and shortened in others (Fig. 4B, asterisks and brackets, respectively) and that flagella were often wrapped around the sperm head (Fig. 4F, J). Interestingly, the connecting piece characteristic of WT sperm (Fig. 4C, arrow) was not identifiable in KO sperm (Fig. 4D–F).

The ultrastructure of WT and KO sperm was also examined following detergent treatment to remove the plasma membrane (Fig. 4G–J). Sperm have a low cytosolic volume and the plasma membrane lies in close association with the acrosome, nucleus, and flagellum such that WT intact (Fig. 4C) and WT detergent treated sperm (Fig. 4G) looked remarkably similar. Characteristic features of WT sperm (indicated in Fig. 4G', magnified view of 4G) include the ventral spur (VS), dorsal lobe (DL), ventral angle (VA), apical hook (AH), and flagellar connecting piece (FCP). The posterior edge of the sub-acrosomal region (SAR) is the limit of the equatorial segment (ES). Detergent treatment of KO sperm revealed a range of underlying structural defects (Fig. 4H–J). Some KO sperm exhibited minor changes in morphology (Fig. 4H), while most had major defects (Fig. 4I and 4J). With the exception of the flagellar principal piece, the occasionally observed nuclear pore complexes (NPCs) and a roughly falciform shape in only the least affected sperm (visualised in Fig. 4H', magnified view of 4H'), well-defined sperm features were absent from KO sperm. In addition to nuclear shaping defects, the SAR, ES, and FCP were conspicuously absent from KO sperm (Fig. 4H–J and H'). Notably, these KO sperm also contained aberrant fibers in the head region (arrowheads, Fig. 4H–J and H') which were not observed in WT sperm. Furthermore, the aberrant fibers observed by SEM in demembranated (Fig. 4H–J, arrowheads), but not in intact (Fig. 4D–F) KO sperm, were also visible by TEM within the plasma membrane of sectioned KO sperm (Fig. 4L, arrowheads). Together, these data indicate that ACTL7B-null epididymal sperm have severe structural defects in the flagellum, particularly in the connecting piece and midpiece regions.

Flagellar proteins contribute to aberrant fibers in Actl7b KO sperm heads

We next investigated the identity of the aberrant fibers in the KO sperm head. Because of the disrupted flagellar midpieces

A

Actl7b Genotype	Mated Males	No. of Litters	Litter Size	No. Fertile
WT	10	38	6.8 ± 0.37*	10
KO	10	0	0	0

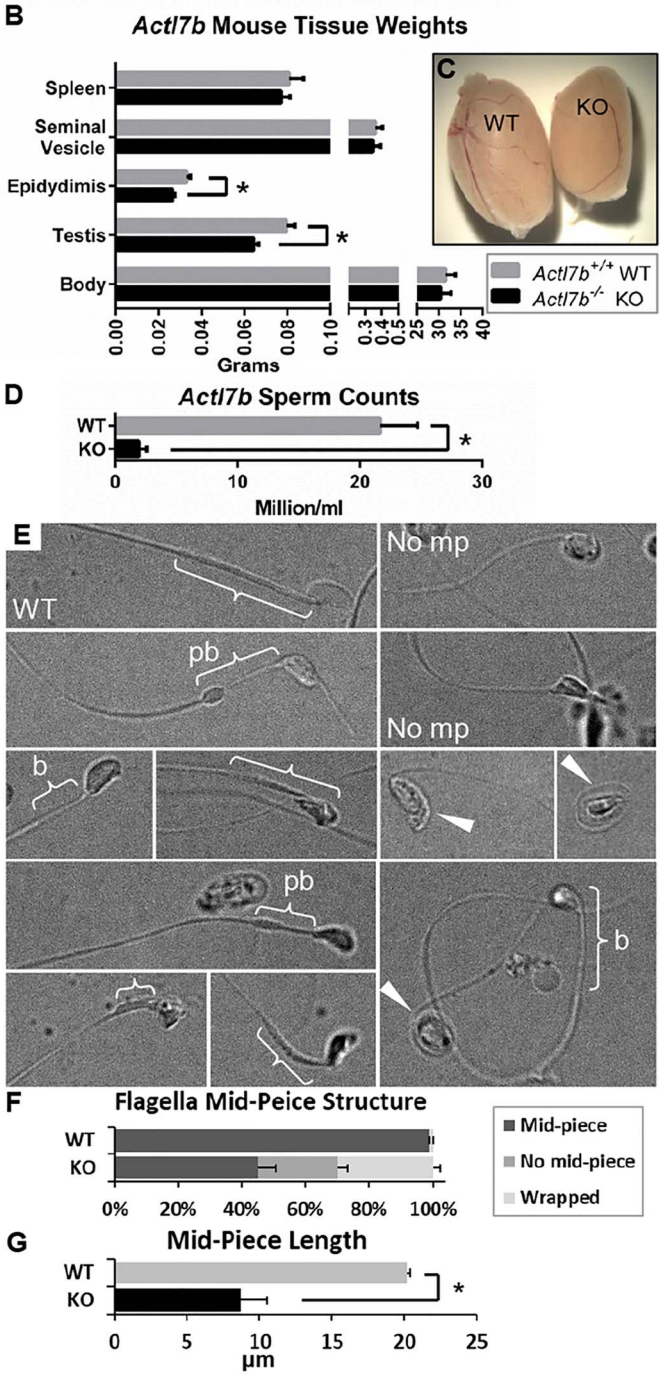

Figure 3. *Actl7b* KO mice are infertile and produce sperm exhibiting OAT with multiple morphological flagellar abnormalities. (A) In sum ,10 KO and 10 WT male mice were mated individually with two WT females, and resulting litter numbers and sizes are indicated. (B) Average body and tissue weights of WT and KO males are compared. (C) Testes from WT and KO mice. (D) Average sperm counts for WT and KO mice. (E) Examples of morphology representative of WT and KO sperm observations. Brackets are indicating lengths of midpiece regions from observable base of head region to initial flagellar principal piece region, No mp = no midpiece, pb = partially bare indicating portions of the observable midpiece appear to be lacking a mitochondrial sheath, b = bare midpiece with no apparent mitochondrial sheath. (F) Average percent of sperm with or without midpiece segments of the flagella, or with flagella wrapped around the head region. (G) Average length of flagella in WT and KO sperm samples. Averages reported ±SEM, and asterisks indicate statistical significance ($P < 0.01$).

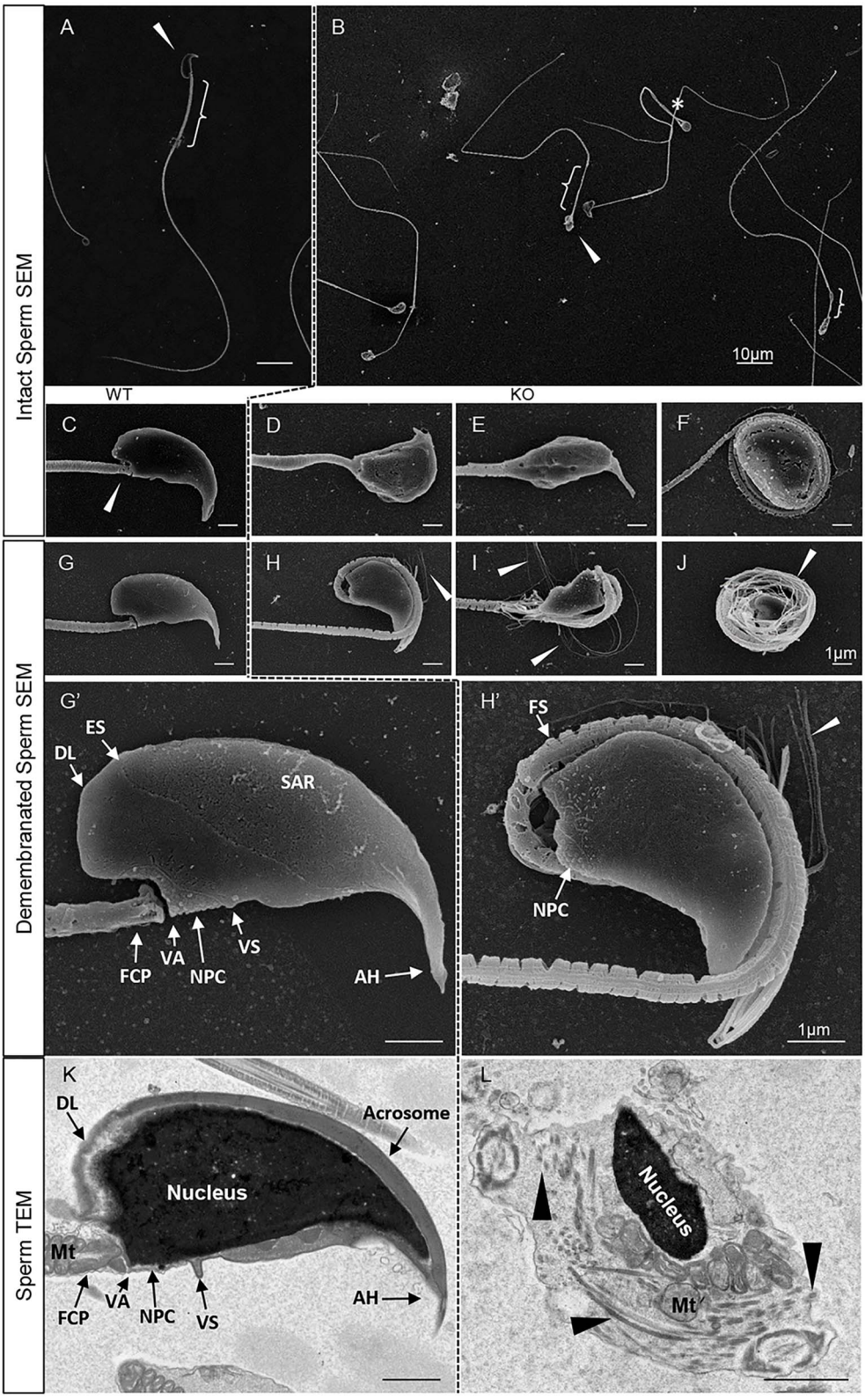

Figure 4. SEM of KO sperm reveals severe and variable teratozoospermia. (A) WT and (B) KO sperm visualised by SEM with the midpiece indicated by a bracket when present or with an asterisk when absent. Arrowheads indicate head region. (C–F) Comparison of the head regions of intact sperm at higher magnification shows the variability in morphology of representative KO sperm (D–F) compared with WT sperm (C, arrowhead indicates connecting piece region). (G–J) Detergent demembranated KO (H–J) and WT (G) sperm reveals sub-membranous structures with aberrant fibers in the head region of KO sperm (H–J, arrowheads). (G') enlarged view of WT sperm in G. (H') enlarged view of sperm in H. (K) WT and (L) KO sperm visualised by SEM. Arrowheads indicate aberrant fibers. AH = apical hook, DL = dorsal lobe, ES = limit of attachment site of equatorial segment, FCP = flagellum connecting piece, FS = fibrous sheath, Mt = mitochondria, NPC = nuclear pore complex, SAR = sub-acrosomal region, VA = ventral angle, VS = ventral spur. Scale bars in A and B are 10 μm, (C)–(L) are each 1 μm.

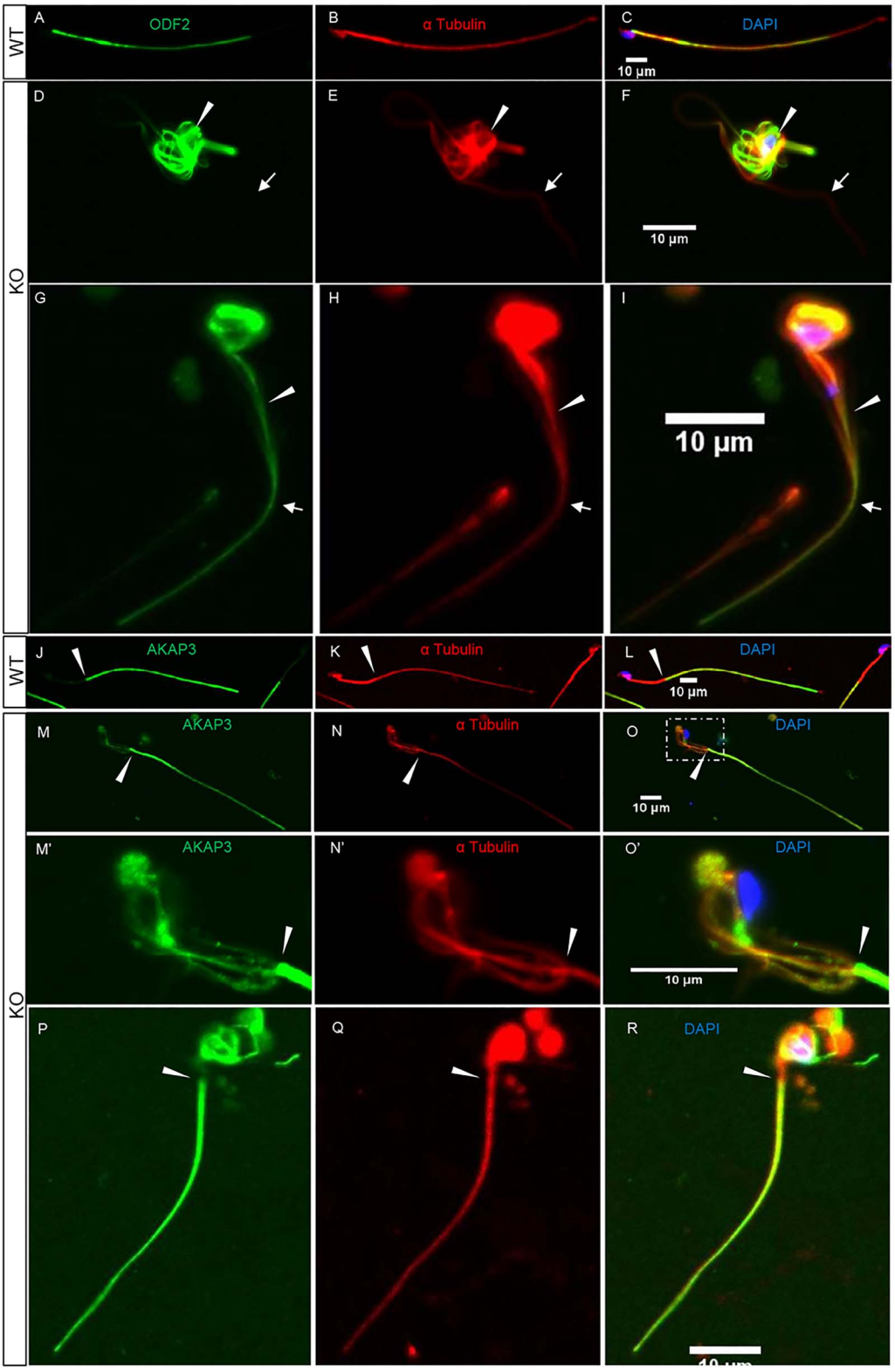

Figure 5. Flagellar protein localisation confirms Multiple Morphological Abnormalities of the Flagella (MMAF) in KO sperm. Cytoskeletal proteins localised to specific regions in WT (A–C and J–L) and KO (D–I and M–R) sperm from the cauda epididymis. (A) ODF2 and (B) alpha tubulin are localised along the midpiece and principal piece regions of the single linear flagellum in WT sperm. (C) is merged WT ODF and tubulin signals with DAPI nuclear staining. In KO sperm, ODF2 (D and G) and tubulin (E and H) are present in the length of the flagellum (arrows D–I) with an apparent multiplication or splaying of fibers in the midpiece (arrowheads D–I) and head region (indicated by DAPI nuclear staining in the merged panel) (F and I). AKAP3 is localised to the fibrous sheath in WT (J) and KO (M and P) and also is present in the head region of KO sperm (region indicated in O magnified in M'–O' with DAPI staining included in O'). Alpha tubulin is localised to the axoneme along the length of the flagellum in WT (K) and KO (N and Q) sperm and is also present in the KO sperm (N and Q) in the disrupted midpiece and head regions. The head region of KO sperm in (M)–(O) is enlarged in (M')–(O') (boxed region shown in O) to show the fiberous nature of aberrantly localised sperm flagellar proteins. The region of the flagellar annulus is indicated with arrowheads in (J)–(R). Scale bars = 10 μm.

and connecting pieces, we posited that the aberrant fibers were composed of flagellar proteins. To test this prediction, we used specific antibodies to known flagellar proteins (Fig. 5 and Supplementary Figs S2 and S3). The normal arrangement of flagellar components in WT sperm was demonstrated using key flagellar markers (Fig. 5A–C and J–L). Alpha tubulin is a major component of the axonemal core microtubules seen extending the full length of the WT flagellum (Fig. 5B and K). The surrounding outer dense fibers (ODFs) containing ODF2 protein were present in the midpiece and principal piece segments of the flagellum (Fig. 5A). In KO sperm showed, ODF2 (Fig. 5D and G, additional examples in Supplementary Fig. S3) and alpha tubulin (Fig. 5E and H) were mislocalised to both the single linear flagellar principal piece (arrows) and to multiplied fiber-like components in the midpiece and head region (indicated by DAPI staining of nuclei in the merged image, Fig. 5F). This is in stark contrast to the rather uniform ODF2 staining in the flagellum, and tubulin localisation in the flagellum and post-acrosomal sheath observed in the WT sperm head lacking fibrous structures. To investigate the contribution of fibrous sheath proteins to aberrant fibers, we localised the major sheath protein A-kinase anchor protein 3 (AKAP3) which in WT sperm was restricted to the fibrous sheath region (Fig. 5J and L). In KO sperm, AKAP3 localised to the aberrant fibers surrounding the head region (Fig. 5M and P with head region of M magnified in M', additional examples in Supplementary Fig. S2). These observations support the hypothesis that the aberrant fibers observed in the KO are composed of flagellar proteins.

Defects in Actl7b KO sperm flagella become apparent during epididymal maturation

We next compared the structure of WT and KO sperm from the cauda epididymis by TEM to define which flagellar components were disrupted by the absence ACTL7B. Cross-sections through the midpiece of WT (Fig. 6A) and KO sperm (Fig. 6B), defined by the presence of the mitochondrial sheath, showed that mitochondria in KO sperm appeared to be abnormally arranged. However, KO sperm usually contained an axonemal complex and ODFs similar to those in WT sperm. Sections through the principal piece region of WT (Fig. 6C) and KO sperm (Fig. 6D) showed that both contain an axoneme with the characteristic 9 + 2 arrangement, ODFs, and fibrous sheath.

Comparisons by SEM of sperm from the cauda epididymis of WT (Fig. 6E) and KO mice (Fig. 6F-G) showed that although the mitochondrial sheath, fibrous sheath, and annulus were present in both genotypes, the connection between the mitochondrial sheath and annulus was lost in some KO sperm. Mitotracker staining showed that mitochondria in KO sperm often were clustered (Fig. 7B and C) rather than forming the typical spiral pattern over the length of the midpiece as seen in WT sperm (Fig. 7A'). Only 2.4% of KO sperm showed a mitochondrial distribution similar to WT sperm (Fig. 7C). Thus, the vast majority (97.6%) of sperm had mitochondria in disorganised clumps on the midpiece (14.7%), in the midpiece and head regions (6.6%), in the head region only (45.7%), or altogether absent (30.5%).

It was shown that F-actin is a component of intermitochondrial cement [47]. To determine whether the lost mitochondrial sheath integrity in ACTL7B KO sperm was accompanied by disruption of F-actin in the mitochondrial sheath, we

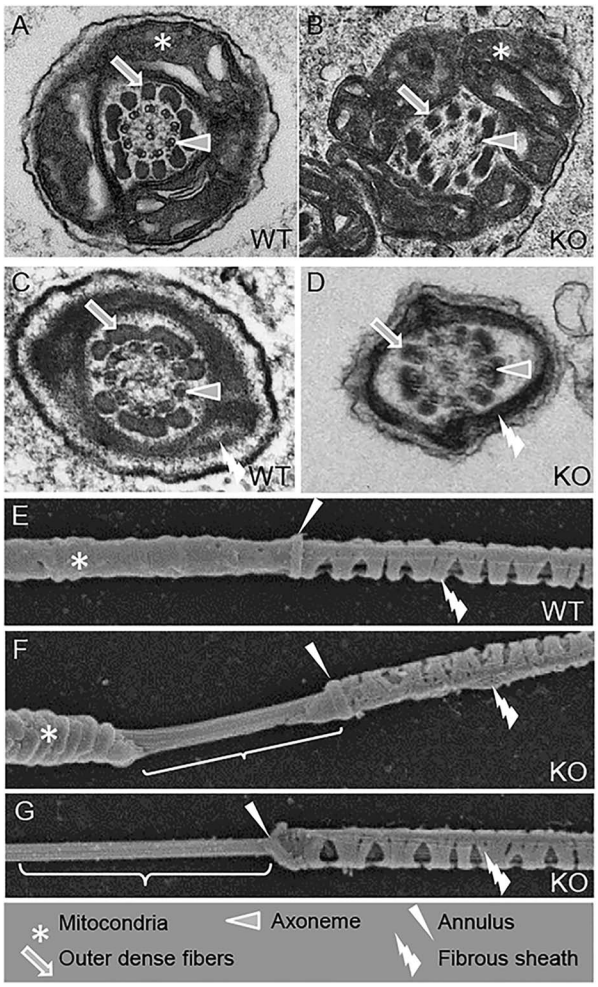

Figure 6. Variable MMAF includes examples of only mildly deviant flagella in the *Actl7b* KO epididymis. Cross-sections through the midpieces of epididymal sperm flagella are viewed by TEM in WT (A) and KO (B); axoneme (arrow head), ODFs (arrow) and mitochondrial sheath (star). Cross-sections of principal piece regions of WT (C) and KO (D) sperm also have the fibrous sheath indicated (bolt). SEM of the central portion of the flagellum where principal and midpiece segments meet for WT (E) and KO (F and G) sperm; mitochondria (star), annulus (arrowhead), fibrous sheath (bolt), bare midpieces lacking mitochondria (bracket).

stained with fluorophore-conjugated phalloidin (Fig. 7 D'–G'). We detected phalloidin-labeled F-actin in the mitochondrial sheath region in WT sperm (Fig D′, arrowhead). However, F-actin was weakly detectable (Fig. 7E'–G', arrowheads) in KO sperm where midpiece segments retained a mitochondrial sheath (as visualised by brightfield in D–G) but was not detectable in KO sperm midpiece segments in regions where mitochondria were absent from the midpiece (Fig. 7E'–G', arrows). Together, this reveals that ACTL7B was not strictly required for formation of these F-actin structures.

To determine when aberrant fibers and flagellar defects arose during spermiogenesis, condensing spermatids were examined by TEM (Fig. 8). In both WT (Fig. 8A) and KO (Fig. 8B) spermatids, structures of the flagellar connecting piece including the basal plate (BP), capitulum (Cp), and segmented columns (SC) were observed. However, the capitulum and centriolar vault appeared diminished. Comparison of the axoneme (Ax), ODFs, and mitochondria (Mt) in flagellar midpieces in spermatids from WT (Fig. 8A) with KO (Fig. 8B and D) mice revealed that KO sperm exhibited both

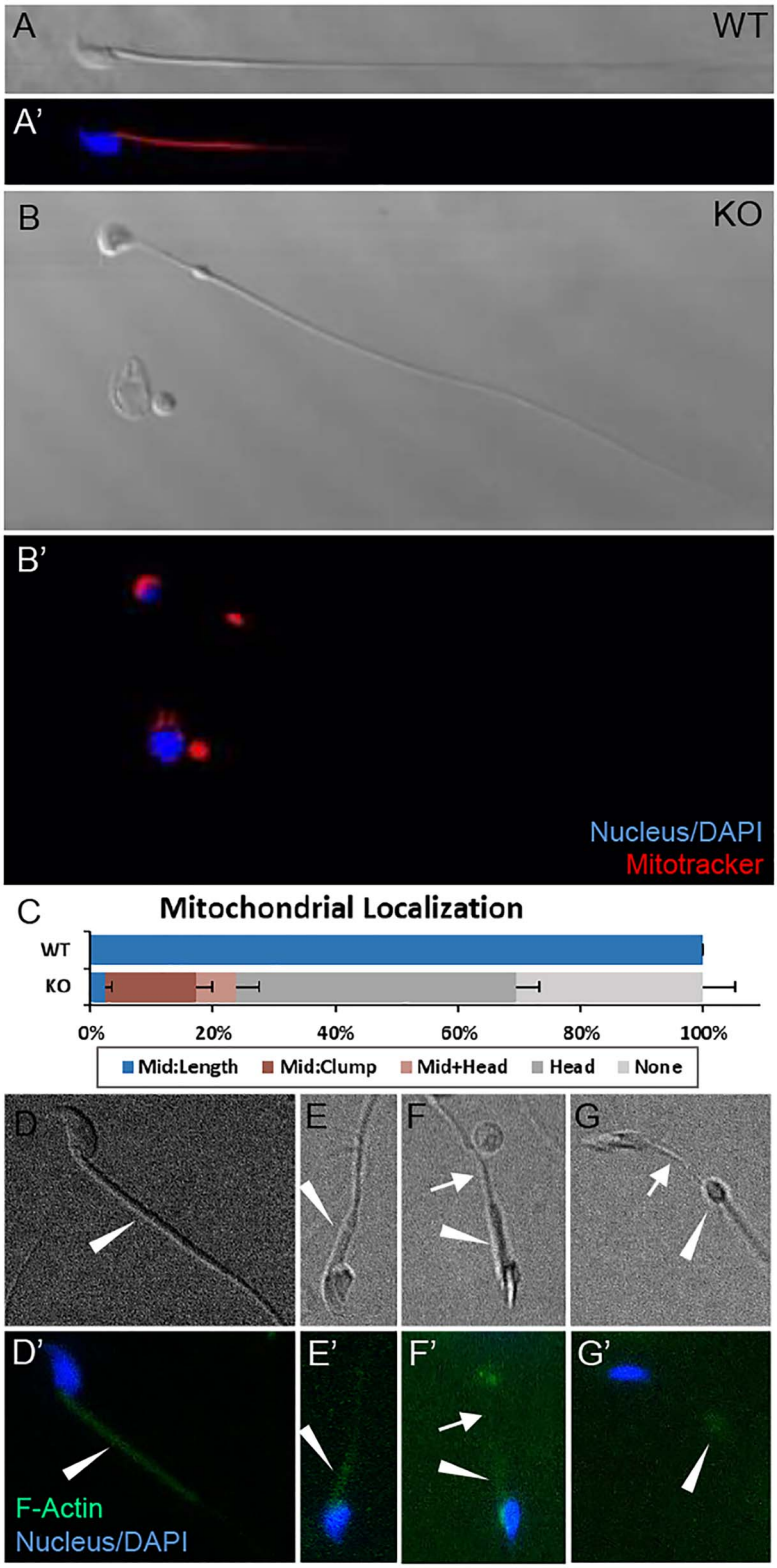

Figure 7. Variable MMAF includes mitochondrial and F-actin localisation defects. MitoTracker dye-stained WT (A') and KO (B') representative sperm with corresponding DIC images (A and B). (C) The localisation of mitochondria were quantitatively classified as normally distributed in the midpiece (Mid:Length), clumped in the midpiece (Mid:Clump), localised to the head region (Head), localised to the head and as clumps or along the midpiece regions (Mid + Head), or as absent altogether (None). For quantitation, at least 200 sperm were scored per biological replicate with $n = 3$ per genotype. F-actin is detectable in the mitochondrial cement region of WT sperm (D', arrowhead). In KO sperm, weak F-actin is detectable (arrowheads in E'–G') in areas where mitochondria are indicated by brightfield morphology (E–G), but not in regions of KO flagella where midpieces are bare/lack the mitochondrial sheath (arrows).

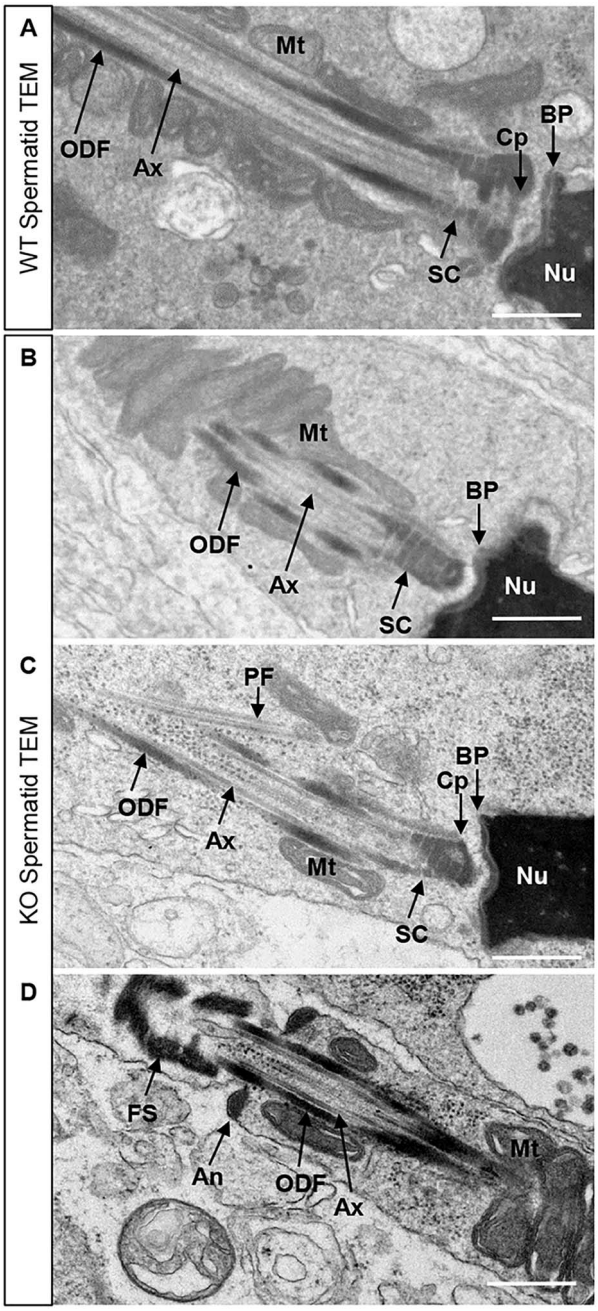

Figure 8. Spermatid flagella in *Actl7b* KO testes appear grossly normal, a few exhibiting minor defects. TEM of spermatids in late steps of development in WT (A) and KO (B–D) testes. (A) WT spermatid connecting piece. (B) Apparently normal KO spermatid connecting piece. (C) KO spermatid connecting piece with an axonemal protofilament (PF) separated from the connecting piece. (D) KO spermatid flagellum exhibiting apparently normal region of transition from midpiece to connecting piece including the annulus. An = annulus, Ax = axoneme, BP = basal plate, Cp = capitulum, Mt = mitochondria, Nu = nucleus, ODF = outer dense fibers, PF = protofilament, SC = segmented columns. Scale bars = 0.5 μm.

organised (Fig. 8B and D) and abnormal (Fig. 8C) midpieces. The abnormal midpieces in KO sperm contained axonemal protofilaments separate from but adjacent to the flagellum (see PF, in Fig. 8C). Of note, aberrant fibers were not observed in the head region of these late-stage condensed spermatids suggesting the flagellar components in the head region of KO sperm appeared during epididymal transit coinciding with sperm maturation and acquisition of motility rather than initial mislocalisation during flagellar development.

Germ cell apoptosis was increased in Actl7b KO testes

The reduced sperm counts in KO mice suggested an increase in cell death. To assess this, TUNEL assays were performed on testis and epididymis sections. Few TUNEL+ cells were observed in the epididymides of WT mice (Fig. 9A). In contrast, numerous TUNEL+ cells, including many round cells, were observed in the epididymides of KO mice (Fig. 9B). To further assess the composition and viability of cells in the epididymal lumina, WT (Fig. 9C, C') and KO (Fig. 9D, D') sections of epididymides were examined by TUNEL staining. WT epididymides contained sperm with normal morphology (Fig. 9C) and occasional TUNEL+ cells (Fig. 9C', green). In KO epididymides, many cells were rounded (Fig. 9D) and many had the appearance round spermatids. KO sperm exhibited abnormal morphology, and abundant cellular debris was present (dashed-line circle in Fig. 9D). All of the rounded cells were TUNEL+ (arrowheads, Fig. 9D') as were many of the sperm (arrows), Fig. 9D'). The percentage of TUNEL+ cells was determined (Fig. 9E) with distinctions made between cells recognisable as sperm (those with flagella and DAPI-stained nuclei), and "other" cells (DAPI-stained nuclei, but no flagella). In the KO samples, "other" cells accounted for ~50% of the cells in the epididymal lumina, whereas, in the WT and Het samples, this population of "other" cells were < 2%. All of the "other" cells for all genotypes were TUNEL+ (Fig. 9E and B). In the WT and Het samples, >92% of sperm were TUNEL-. KO sperm (blue and dark grey portions of the KO bar graph in Fig. 9E) were ~ 60% TUNEL-. When the "other" cells in the KO were included in the TUNEL counts, only ~28% of cells were TUNEL- (Fig. 9E).

To assess whether cell death was initiated during spermiogenesis within the seminiferous epithelium, TUNEL staining was performed on WT and KO testis sections (Fig. 9F and G, respectively). Few TUNEL+ cells were observed near the basement membrane in both WT and KO mouse testes (dark brown staining). In KO testes, rounded TUNEL+ cells were observed near the lumina of seminiferous tubules (Fig. 9G, arrowheads). This revealed germ cell loss in the testis contributed to the reduced epididymal sperm counts in KO mice. These sloughed cells were the likely source of the abundant TUNEL+ rounded cells in the epididymal lumina (Fig. 9B–D'). The abnormal seminiferous epithelia in KO testis also suggest germ cell sloughing into the lumina (Fig. 9I). As TUNEL staining indicated that condensing spermatids near the luminal surface were TUNEL+, we also examined chromatin compaction utilising CMA3 staining assays (Fig. 9H). Results revealed both WT and Het mouse sperm exhibited <5% CMA3+ sperm, while KO ~ 25% of KO sperm were CMA3+ (Fig. 9H). This level of significantly compromised chromatin compaction was in a smaller proportion of sperm than those that were TUNEL+, and may be a consequence of cell death rather than an indicator of a role for ACTL7B.

Discussion

Here, we report an essential role for ACTL7B in normal sperm development. As a result of *Actl7b* ablation, mice were infertile with severe and variable teratozoospermia. This condition

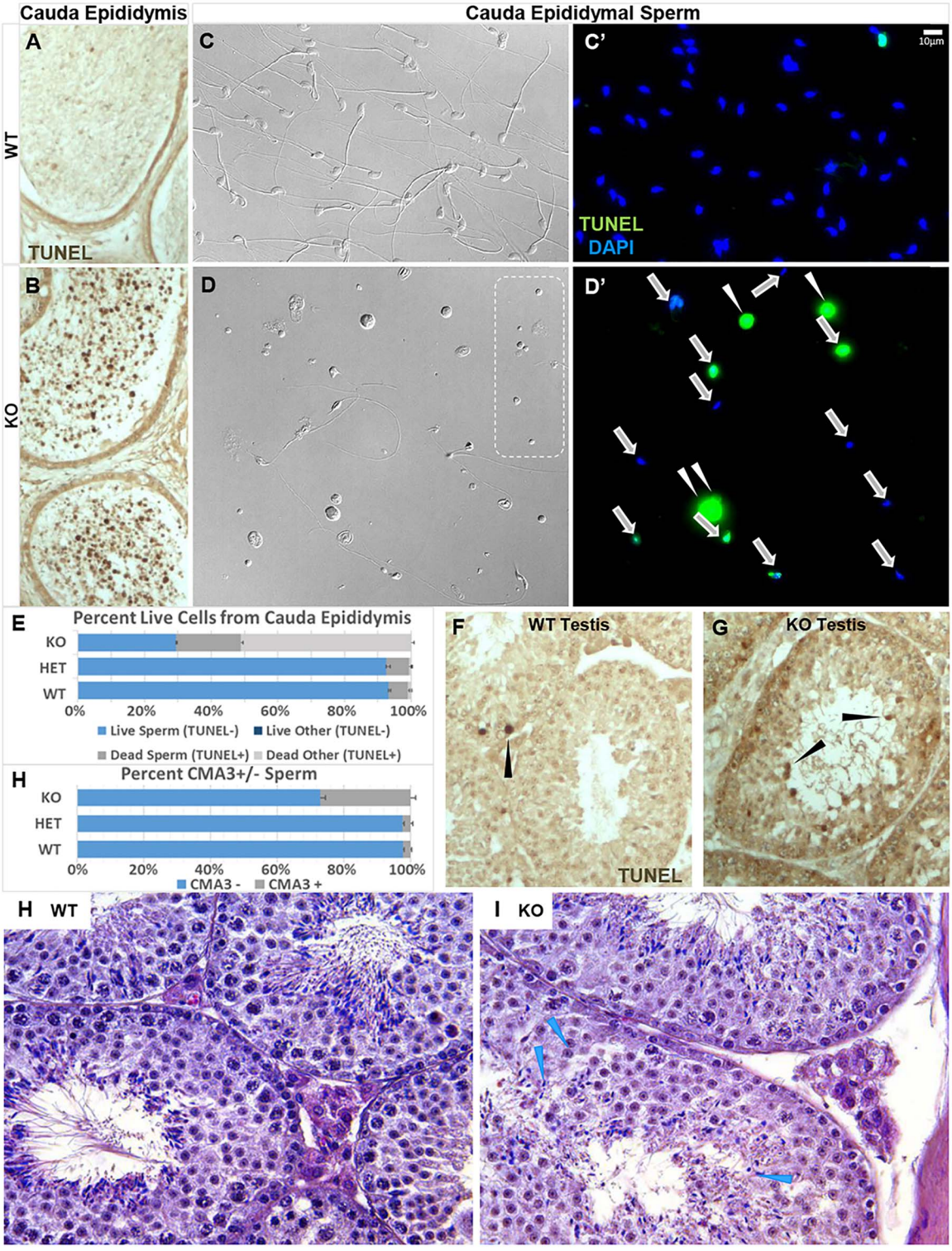

Figure 9. Lack of ACTL7B leads to decreased viability in spermatids and sperm. TUNEL assays on epididymal sections from WT (A) and KO (B) mice. A few TUNEL+ (dark brown) cells are present in the cauda epididymides of WT (A). TUNEL staining is abundant in cauda epididymides of KO mice (B). Whole mount sperm collected from the epididymides and spread on slides from WT (C and C′) and KO (D and D′) mice show the overall cell composition/morphology (C and D, phase contrast) and corresponding TUNEL+ cells (C′ and D′, green = TUNEL, blue = DAPI, Arrows indicate sperm, arrowheads indicate cells classified as "other cells", area inside dashed line in D is representative of DAPI negative debris that is not included in sperm/cell counts). The percent TUNEL+ epididymal cells as seen in (C′) and (D′) is quantified for each genotype (E). At least 200 sperm were scored per biological replicate, and $n = 3$ for each genotype. TUNEL assays on sections of testis from WT (F) and KO (G) mice. A few TUNEL+ cells are present in the basal area of the seminiferous tubules in WT and KO mice and near the luminal surface of KO seminiferous tubules (dark brown, arrowheads). H&E stained histological sections of WT (H), and KO (I) testes, with some areas of seminiferous epithelial disruption observed in KO (arrowheads).

is characterised by decreased sperm counts and decreased sperm motility, a combination of defects termed Oligoasthenoteratozoospermia (OAT). Our data reveal a requirement for ACTL7B in structural integrity of the connecting piece, axoneme, and mitochondrial sheath of the spermatid flagellum, and for secure association of ODFs, axonemal protofilaments, and mitochondria. The phenotypic similarities seen with mutations in genes for actin capping proteins and of actin capping interacting proteins strongly suggests the observed defects are mediated by regulation of novel actin-associated complexes localised to these regions, impacting morphogenesis and maturation. This defined requirement for ACTL7B in spermiogenesis and male fertility also expands the known roles of the ARP family to include male fertility and flagellar structural integrity.

Many of the general defects we observed in *Actl7b* KO sperm are commonly seen in genetic models of male infertility, and it is therefore important to focus on unique aspects of phenotypes for a particular genetic model to better understand what can be learned about the function of specific gene products. With the largest number of tissue specific expressed genes [7, 48], this is especially true in models of testis biology in which highly specialised and complex cellular processes are required for the production of sperm. Furthermore, spermiogenesis is a highly spatiotemporally coordinated cellular morphogenic program that involves interconnected changes in spermatid cytoskeletal structures, organelle biogenesis and function, transcription, translation, nuclear and cellular shaping, chromatin structural changes and condensation, and intracellular transport [22, 49, 50]. Such connectivity and interdependence of functions for morphogenesis might explain why targeted mutations in genes expected to play diverse roles in cell biology, have resulted in similar-appearing spermatid defects [39, 40, 51–71]. Examples include disruptions to the function of intracellular transport mechanisms [54, 56, 66, 68], organelle biogenesis [60, 65, 67], and transcription or translation [62, 63] that manifest as structural defects in spermatids and sperm with overlapping phenotypes such as retained cytoplasm, nuclear- and cell-shaping defects, and reduced sperm motility. Therefore, detailed observation is required to identify rare defects that can lend insight into the function of individual molecules and mechanisms in spermiogenesis. Among the constellation of defects observed in teratozoospermic *Actl7b* KO mouse sperm, we focus here on a unique aberration in sperm flagellar integrity.

A key finding reported here for the *Actl7b* KO mouse sperm are the severe flagellar defects and specific destabilisation of the sperm flagellum, which are uncommon in models of infertility. In *Actl7b* KO sperm, we find a conspicuous absence of the flagella connecting pieces including capitulum and segmented columns, the nuclear-associated basal plate where the flagella connecting piece attaches to the sperm flagellum, and severe disruptions in flagellar midpiece structure. Despite these observations in epididymal sperm, the affected structures appear relatively morphologically normal in testicular sperm, indicating flagellar components could form and assemble in the absence ACTL7B. However, the disintegration of these structures in all observed *Actl7b* KO sperm by the time they reach the cauda epididymis suggest that the integrity of the connecting and midpiece structures were compromised, allowing for lost integrity during epididymal transit.

Evidence of a role for actin in epididymal sperm maturation was previously inferred from observations of localisation of actin and actin-interacting proteins. In sperm, actin has been localised to the sperm connecting piece, mitochondrial sheath, and transiently to the flagellum after spermiation and prior to epididymal maturation [20, 47, 72, 73]. Actin and actin binding proteins were also identified as candidate sperm maturation factors through proteomics [74]. Interestingly, during sperm maturation in the epididymis, the stiffness of the flagellar midpiece is reduced [75]. At this time, connections of the ODFs to the mitochondrial sheath are lost and the ODFs become free to slide relative to each other under the action of dynein motors in the flagellum [76, 77]. In the context of these previous reports, our observations that mitochondria localisation and flagellar midpiece integrity are compromised in sperm that have transited the epididymis seem to suggest a disruption in structural flagellar midpiece integrity with consequences visible after mitochondrial release from ODFs during sperm maturation. This indicates a potential as-yet-unidentified disruption in the intermitochondrial cement disrupting the mitochondrial sheath integrity. Results from studies to artificially disrupt the mitochondrial sheath have shown that it provides necessary structural support to prevent the axoneme and ODFs from buckling under the forces associated with flagellar motion [78–84]. In these studies, when the mitochondrial sheath was disrupted in sperm, and motility was induced thereby inflicting mechanical force, the ODFs and axoneme separated from each other, but the ODFs remained secured at the connecting piece. In *Actl7b* KO sperm, we observed that the axoneme in the midpiece appeared to separate in a similar way. However, we also observed the loss of connecting piece integrity, indicating a secondary role for ACTL7B in flagellar connecting piece integrity.

Interestingly, in rat and mouse sperm, the basal body that nucleates flagellogenesis is largely disassembled prior to sperm maturation [85–87]. Thus, the axoneme is not anchored by the basal body in sperm as it is in other flagella and cilia. Instead, it is the ODFs that are anchored at the segmented columns of the connecting piece, each of which, in turn, secures an axonemal doublet [88–90]. In *Actl7b* KO mice, the segmented columns and basal plate were formed in testicular sperm. However, the ODFs appeared to dissociate thereafter, not only from each other as noted above, but also from the connecting piece, which was no longer detectable in epididymal KO sperm. This ultimately led to shortened or absent midpieces. It is of note that a few factors involved in connecting piece stability have been identified [91]. Of interest, the testis-specific spermatogenesis and centriole associated one like (SPATC1L) protein interacts with and phosphorylates "capping actin protein of muscle Z-line subunit beta" (CAPZB). *Spatc1l* KO sperm exhibited fragile connecting pieces leading to head-tail dissociations after spermiation, but flagellar midpieces appeared to maintain their integrity [91]. This suggests a potential role for actin regulatory proteins in the stability of sperm flagella connecting pieces. Our observation that ACTL7B is also required to ensure the structural integrity of the connecting piece provides further evidence for a key role for ARPs.

Within the actin-related family of proteins, only conventional actins (alpha, beta and gamma actin) form dynamic filamentous actin [32, 92]. Other ARPs are involved in diverse functions such as ARP1 and ARP11 contributions to dynein-dynactin complexes where ARP1 forms a short filament within the complex [31, 93], ARP2 and ARP3 contributions to F-actin nucleation and branching complexes [92], and ARP5 and ARP9 contributions to chromatin remodeling complexes

in somatic cells [30, 94–97]. Each of these non-conventional roles of the broader ARP family requires that the ARP proteins form large multimeric protein complexes. Given that our data indicate ACTL7B is not required for F-actin formation in the mitochondrial sheath, we propose that ACTL7B does not function as a monomeric filament forming conventional actin, but rather forms a novel multimeric protein complex like the other non-conventional ARPs. ACTL7B, perhaps in such a novel multi-protein complex, is required for mediating structural integrity and attachment of flagellar components in sperm; specifically, the association of axoneme and ODF to the capitulum of the flagellar connecting piece and along the length of the flagellar midpiece for the stability of connecting piece, protofilament, and mitochondrial associations. We propose that given the known roles of CAPZB and SPATC1L, that the ACTL7B containing complex may also contain actin capping protein CAPZB and may be in part under regulatory control of SPATC1L phosphorylation to provide structural support for axonemal protofilament and ODF associations in the capitulum and along the midpiece of sperm flagella.

One of the most apparent defects in *Actl7b* KO sperm was the presence of aberrant fibers containing flagellar proteins in the head region. We propose that these ODF2 and tubulin containing aberrant fibers are composed of degraded flagellar axoneme and ODFs which collapsed back toward the sperm head within the sperm plasma membrane. The observation of fibrous sheath protein AKAP3 co-localisation to these fibers is not as easily explained as the fibrous sheath of the KO epididymal sperm appear to maintain relatively normal structure. An alternate interpretation is that the flagellar ODF and axoneme dissembled and reformed fibrous structures *de novo* in the aberrant locations. In either case, we conclude that the structural integrity of the flagellum was compromised in *Actl7b* KO sperm, ultimately leading to the disruption of the integrity and organisation of the connecting and midpiece segments and formation of observed aberrant fibers. To our knowledge, the only other reports of genetic models reported to cause such fibers were in the ENU-induced repro32 mutant that had a defect in the spermatid-specific actin capping protein CAPZA3 [40] and in the KO mouse for protein kinase HIPK4, which phosphorylates actin modulating proteins and may be required for actin capping protein localisation [98]. In *Hipk4* KO mice, ~75% of sperm flagella were abnormal, and aberrant fibers in the head region of some sperm were identified as axonemal components [98]. In *repro32* mutant mice, sperm exhibited aberrant fiber localisation to the head region identified to include ODFs [40]. Aberrant fiber formation specifically in mutant sperm from sterile mouse models containing a mutation in actin caping protein *Capza3,* the *Hipk4* kinase known to modulate actin dynamics, or with deletion of the ARP *Actl7b,* strongly supports an essential role for actin regulation in spermiogenesis required to establish the integrity of sperm flagella. Studies are ongoing to investigate ACTL7B roles during spermiogenesis and define the interaction of ACTL7B with cytoskeletal and cytoskeletal regulating proteins critical for spermatid morphogenesis.

Acknowledgments

We thank Linwood Koonce (NIEHS) for his assistance with animal colony maintenance and Victoria Madden (University of North Carolina Chapel Hill Microscopy Services Laboratory) for her expert technical assistance with EM sample preparation.

Supplementary Material

Supplementary material is available at *BIOLRE* online.

Conflict of interest

The authors declare no conflicts of interest.

References

1. Finer LB, Zolna MR. Unintended pregnancy in the United States: incidence and disparities, 2006. *Contraception* 2011; **84**:478–485.
2. Skakkebaek NE, Jorgensen N, Main KM, Meyts ERD, Leffers H, Andersson AM, Juul A, Carlsen E, Mortensen GK, Jensen TK, Toppari J. Is human fecundity declining? *Int J Androl* 2006; **29**: 2–11.
3. Pierik FH, van Ginneken AM, Dohle GR, Vreeburg JTM, Weber RFA. The advantages of standardized evaluation of male infertility. *Int J Androl* 2000; **23**:340–346.
4. Eddy EM. Male germ cell gene expression. *Recent Prog Horm Res* 2002; **57**:103–128.
5. Eddy EM. 'Chauvinist genes' of male germ cells: gene expression during mouse spermatogenesis. *Reprod Fertil Dev* 1995; **7**: 695–704.
6. Hermann BP, Cheng K, Singh A, Roa-de la Cruz L, Mutoji KN, Chen IC, Gildersleeve H, Lehle JD, Mayo M, Westernströer B, Law NC, Oatley MJ *et al.* The mammalian spermatogenesis single-cell transcriptome, from spermatogonial stem cells to spermatids. *Cell Rep* 2018; **25**:1650–1667.e8.
7. Sonawane AR, Platig J, Fagny M, Chen CY, Paulson JN, Lopes-Ramos CM, DeMeo DL, Quackenbush J, Glass K, Kuijjer ML. Understanding tissue-specific gene regulation. *Cell Rep* 2017; **21**: 1077–1088.
8. Castaneda JM, Hua R, Miyata H, Oji A, Guo Y, Cheng Y, Zhou T, Guo X, Cui Y, Shen B, Wang Z, Hu Z *et al.* TCTE1 is a conserved component of the dynein regulatory complex and is required for motility and metabolism in mouse spermatozoa. *Proc Natl Acad Sci USA* 2017; **114**:E5370–E5378.
9. Castaneda JM, Shimada K, Satouh Y, Yu Z, Devlin DJ, Ikawa M, Matzuk MM. FAM209 associates with DPY19L2, and is required for sperm acrosome biogenesis and fertility in mice. *J Cell Sci* 2021; **134**:jcs259206.
10. Nozawa K, Fujihara Y, Devlin DJ, Deras RE, Kent K, Larina IV, Umezu K, Yu Z, Sutton CM, Ye Q, Dean LK, Emori C *et al.* The testis-specific E3 ubiquitin ligase RNF133 is required for fecundity in mice. *BMC Biol* 2022; **20**:161.
11. Nozawa K, Zhang Q, Miyata H, Devlin DJ, Yu Z, Oura S, Koyano T, Matsuyama M, Ikawa M, Matzuk MM. Knockout of serine-rich single-pass membrane protein 1 (Ssmem1) causes globozoospermia and sterility in male micedagger. *Biol Reprod* 2020; **103**: 244–253.
12. Shimada K, Park S, Miyata H, Yu Z, Morohoshi A, Oura S, Matzuk MM, Ikawa M. ARMC12 regulates spatiotemporal mitochondrial dynamics during spermiogenesis and is required for male fertility. *Proc Natl Acad Sci USA* 2021; **118**:E2018355118.
13. Xu Z, Miyata H, Kaneda Y, Castaneda JM, Lu Y, Morohoshi A, Yu Z, Matzuk MM, Ikawa M. CIB4 is essential for the haploid phase of spermatogenesis in micedagger. *Biol Reprod* 2020; **103**: 235–243.
14. Lu Y, Oura S, Matsumura T, Oji A, Sakurai N, Fujihara Y, Shimada K, Miyata H, Tobita T, Noda T, Castaneda JM, Kiyozumi D *et al.* CRISPR/Cas9-mediated genome editing reveals 30 testis-enriched genes dispensable for male fertility in micedagger. *Biol Reprod* 2019; **101**:501–511.
15. Miyata H, Castaneda JM, Fujihara Y, Yu Z, Archambeault DR, Isotani A, Kiyozumi D, Kriseman ML, Mashiko D, Matsumura T, Matzuk RM, Mori M *et al.* Genome engineering uncovers 54 evolutionarily conserved and testis-enriched genes that are not required for male fertility in mice. *Proc Natl Acad Sci USA* 2016; **113**:7704–7710.

16. Oyama Y, Miyata H, Shimada K, Fujihara Y, Tokuhiro K, Garcia TX, Matzuk MM, Ikawa M. CRISPR/Cas9-mediated genome editing reveals 12 testis-enriched genes dispensable for male fertility in mice. *Asian J Androl* 2022; **24**:266–272.
17. Park S, Shimada K, Fujihara Y, Xu Z, Shimada K, Larasati T, Pratiwi P, Matzuk RM, Devlin DJ, Yu Z, Garcia TX, Matzuk MM *et al.* CRISPR/Cas9-mediated genome-edited mice reveal 10 testis-enriched genes are dispensable for male fecundity. *Biol Reprod* 2020; **103**:195–204.
18. Sun J, Lu Y, Nozawa K, Xu Z, Morohoshi A, Castaneda JM, Noda T, Miyata H, Abbasi F, Shawki HH, Takahashi S, Devlin DJ *et al.* CRISPR/Cas9-based genome editing in mice uncovers 13 testis- or epididymis-enriched genes individually dispensable for male reproductiondagger. *Biol Reprod* 2020; **103**:183–194.
19. Brener E, Rubinstein S, Cohen G, Shternall K, Rivlin J, Breitbart H. Remodeling of the actin cytoskeleton during mammalian sperm capacitation and acrosome reaction. *Biol Reprod* 2003; **68**: 837–845.
20. Clarke GN, Clarke FM, Wilson S. Actin in human spermatozoa. *Biol Reprod* 1982; **26**:319–327.
21. Halenda RM, Primakoff P, Myles DG. Actin filaments, localized to the region of the developing acrosome during early stages, are lost during later stages of Guinea pig spermiogenesis. *Biol Reprod* 1987; **36**:491–499.
22. Kierszenbaum AL, Rivkin E, Tres LL. Acroplaxome, an F-actin-keratin-containing plate, anchors the acrosome to the nucleus during shaping of the spermatid head. *Mol Biol Cell* 2003; **14**: 4628–4640.
23. Masri BA, Russell LD, Vogl AW. Distribution of actin in spermatids and adjacent Sertoli cell regions of the rat. *Anat Rec* 1987; **218**: 20–26.
24. Sun X, Kovacs T, Hu YJ, Yang WX. The role of actin and myosin during spermatogenesis. *Mol Biol Rep* 2011; **38**:3993–4001.
25. Welch JE, O'Rand MG. Identification and distribution of actin in spermatogenic cells and spermatozoa of the rabbit. *Dev Biol* 1985; **109**:411–417.
26. Yagi A, Paranko J. Localization of actin, alpha-actinin, and tropomyosin in bovine spermatozoa and epididymal epithelium. *Anat Rec* 1992; **233**:61–74.
27. dos Remedios CG, Chhabra D, Kekic M, Dedova IV, Tsubakihara M, Berry DA, Nosworthy NJ. Actin binding proteins: regulation of cytoskeletal microfilaments. *Physiol Rev* 2003; **83**:433–473.
28. Bisi S, Disanza A, Malinverno C, Frittoli E, Palamidessi A, Scita G. Membrane and actin dynamics interplay at lamellipodia leading edge. *Curr Opin Cell Biol* 2013; **25**:565–573.
29. Dion V, Shimada K, Gasser SM. Actin-related proteins in the nucleus: life beyond chromatin remodelers. *Curr Opin Cell Biol* 2010; **22**:383–391.
30. Chen M, Shen X. Nuclear actin and actin-related proteins in chromatin dynamics. *Curr Opin Cell Biol* 2007; **19**:326–330.
31. Eckley DM, Gill SR, Melkonian KA, Bingham JB, Goodson HV, Heuser JE, Schroer TA. Analysis of dynactin subcomplexes reveals a novel actin-related protein associated with the arp1 minifilament pointed end. *J Cell Biol* 1999; **147**:307–320.
32. Goodson HV, Hawse WF. Molecular evolution of the actin family. *J Cell Sci* 2002; **115**:2619–2622.
33. Muller J, Oma Y, Vallar L, Friederich E, Poch O, Winsor B. Sequence and comparative genomic analysis of actin-related proteins. *Mol Biol Cell* 2005; **16**:5736–5748.
34. Tanaka H, Iguchi N, Egydio de Carvalho C, Tadokoro Y, Yomogida K, Nishimune Y. Novel actin-like proteins T-ACTIN 1 and T-ACTIN 2 are differentially expressed in the cytoplasm and nucleus of mouse haploid germ cells. *Biol Reprod* 2003; **69**: 475–482.
35. Chadwick BP, Mull J, Helbling LA, Gill S, Leyne M, Robbins CM, Pinkett HW, Makalowska I, Maayan C, Blumenfeld A, Axelrod FB, Brownstein M *et al.* Cloning, mapping, and expression of two novel actin genes, actin-like-7A (ACTL7A) and actin-like-7B (ACTL7B), from the familial dysautonomia candidate region on 9q31. *Genomics* 1999; **58**:302–309.
36. Tondeleir D, Vandamme D, Vandekerckhove J, Ampe C, Lambrechts A. Actin isoform expression patterns during mammalian development and in pathology: insights from mouse models. *Cell Motil Cytoskeleton* 2009; **66**:798–815.
37. Niedenberger BA, Chappell VK, Kaye EP, Renegar RH, Geyer CB. Nuclear localization of the actin regulatory protein Palladin in sertoli cells. *Mol Reprod Dev* 2013; **80**:403–413.
38. McLean DJ. Spermatogonial Stem Cell Transplantation, Testicular Function, and Restoration of Male Fertility in Mice. In: Hou SX, Singh SR (eds.), *Spermatogonial Stem Cell Transplantation, Testiscular Function, and Restoration of Male Fertility in Mice, in Germline Stem Cells*. Totowa, NJ: Humana Press; 149–162.
39. Miki K, Willis WD, Brown PR, Goulding EH, Fulcher KD, Eddy EM. Targeted disruption of the Akap4 gene causes defects in sperm flagellum and motility. *Dev Biol* 2002; **248**:331–342.
40. Geyer CB, Inselman AL, Sunman JA, Bornstein S, Handel MA, Eddy EM. A missense mutation in the Capza3 gene and disruption of F-actin organization in spermatids of repro32 infertile male mice. *Dev Biol* 2009; **330**:142–152.
41. Clement TM, Inselman AL, Goulding EH, Willis WD, Eddy EM. Disrupting cyclin dependent kinase 1 in spermatocytes causes late meiotic arrest and infertility in mice. *Biol Reprod* 2015; **93**:137.
42. Brown PR, Miki K, Harper DB, Eddy EM. A-kinase anchoring protein 4 binding proteins in the fibrous sheath of the sperm flagellum. *Biol Reprod* 2003; **68**:2241–2248.
43. Shao X, Tarnasky HA, Schalles U, Oko R, van der Hoorn FA. Interactional cloning of the 84-kDa major outer dense fiber protein Odf84. Leucine zippers mediate associations of Odf84 and Odf27. *J Biol Chem* 1997; **272**:6105–6113.
44. Russell LD *et al.* (eds.). *Histological and histopathological evaluation of the testis*, 1st ed. Cache River Press: St Louis MO; 1990: 286.
45. Conchie J, Findlay J. Influence of gonadectomy, sex hormones and other factors, on the activity of certain glycosidases in the rat and mouse. *J Endocrinol* 1959; **18**:132–146.
46. Conchie J, Findlay J, Levvy GA. Mammalian glycosidases; distribution in the body. *Biochem J* 1959; **71**:318–325.
47. Gervasi MG *et al.* The actin cytoskeleton of the mouse sperm flagellum is organized in a helical structure. *J Cell Sci* 2018; **131**:jcs215897.
48. Zhu J, Chen G, Zhu S, Li S, Wen Z, Bin Li, Zheng Y, Shi L. Identification of tissue-specific protein-coding and noncoding transcripts across 14 human tissues using RNA-seq. *Sci Rep* 2016; **6**:28400.
49. Kierszenbaum AL, Rivkin E, Tres LL. Cytoskeletal track selection during cargo transport in spermatids is relevant to male fertility. *Spermatogenesis* 2011; **1**:221–230.
50. Kierszenbaum AL, Tres LL. The acrosome-acroplaxome-manchette complex and the shaping of the spermatid head. *Arch Histol Cytol* 2004; **67**:271–284.
51. Mendoza-Lujambio I, Burfeind P, Dixkens C, Meinhardt A, Hoyer-Fender S, Engel W, Neesen J. The Hook1 gene is non-functional in the abnormal spermatozoon head shape (azh) mutant mouse. *Hum Mol Genet* 2002; **11**:1647–1658.
52. Liu Y, DeBoer K, de Kretser DM, O'Donnell L, O'Connor AE, Merriner DJ, Okuda H, Whittle B, Jans DA, Efthymiadis A, McLachlan RI, Ormandy CJ *et al.* LRGUK-1 is required for basal body and manchette function during spermatogenesis and male fertility. *PLoS Genet* 2015; **11**:e1005090.
53. Pierre V, Martinez G, Coutton C, Delaroche J, Yassine S, Novella C, Pernet-Gallay K, Hennebicq S, Ray PF, Arnoult C. Absence of Dpy19l2, a new inner nuclear membrane protein, causes globozoospermia in mice by preventing the anchoring of the acrosome to the nucleus. *Development* 2012; **139**:2955–2965.
54. Akhmanova A, Mausset-Bonnefont AL, van Cappellen W, Keijzer N, Hoogenraad CC, Stepanova T, Drabek K, van der Wees J, Mommaas M, Onderwater J, van der Meulen H, Tanenbaum ME *et al.* The microtubule plus-end-tracking protein CLIP-170 associates with the spermatid manchette and is essential for spermatogenesis. *Genes Dev* 2005; **19**:2501–2515.

55. Khatchadourian K, Smith CE, Metzler M, Gregory M, Hayden MR, Cyr DG, Hermo L. Structural abnormalities in spermatids together with reduced sperm counts and motility underlie the reproductive defect in HIP1−/− mice. *Mol Reprod Dev* 2007; **74**: 341–359.
56. Lerer-Goldshtein T, Bel S, Shpungin S, Pery E, Motro B, Goldstein RS, Bar-Sheshet SI, Breitbart H, Nir U. TMF/ARA160: a key regulator of sperm development. *Dev Biol* 2010; **348**:12–21.
57. Martianov I, Brancorsini S, Catena R, Gansmuller A, Kotaja N, Parvinen M, Sassone-Corsi P, Davidson I. Polar nuclear localization of H1T2, a histone H1 variant, required for spermatid elongation and DNA condensation during spermiogenesis. *Proc Natl Acad Sci USA* 2005; **102**:2808–2813.
58. Rainey MA, George M, Ying GG, Akakura R, Burgess DJ, Siefker E, Bargar T, Doglio L, Crawford SE, Todd GL, Govindarajan V, Hess RA *et al.* The endocytic recycling regulator EHD1 is essential for spermatogenesis and male fertility in mice. *BMC Dev Biol* 2010; **10**:37.
59. Lin YN, Roy A, Yan W, Burns KH, Matzuk MM. Loss of zona pellucida binding proteins in the acrosomal matrix disrupts acrosome biogenesis and sperm morphogenesis. *Mol Cell Biol* 2007; **27**:6794–6805.
60. O'Donnell L, Rhodes D, Smith SJ, Merriner DJ, Clark BJ, Borg C, Whittle B, O'Connor AE, Smith LB, McNally FJ, de Kretser DM, Goodnow CC *et al.* An essential role for katanin p80 and microtubule severing in male gamete production. *PLoS Genet* 2012; **8**:e1002698.
61. Wu AT, Sutovsky P, Xu W, van der Spoel AC, Platt FM, Oko R. The postacrosomal assembly of sperm head protein, PAWP, is independent of acrosome formation and dependent on microtubular manchette transport. *Dev Biol* 2007; **312**:471–483.
62. Xu X, Toselli PA, Russell LD, Seldin DC. Globozoospermia in mice lacking the casein kinase II alpha' catalytic subunit. *Nat Genet* 1999; **23**:118–121.
63. Yap DB, Walker DC, Prentice LM, McKinney S, Turashvili G, Mooslehner-Allen K, de Algara TR, Fee J, de Tassigny X'A, Colledge WH, Aparicio S. Mll5 is required for normal spermatogenesis. *PLoS One* 2011; **6**:e27127.
64. Zheng H, Stratton CJ, Morozumi K, Jin J, Yanagimachi R, Yan W. Lack of Spem1 causes aberrant cytoplasm removal, sperm deformation, and male infertility. *Proc Natl Acad Sci USA* 2007; **104**:6852–6857.
65. Ito C, Suzuki-Toyota F, Maekawa M, Toyama Y, Yao R, Noda T, Toshimori K. Failure to assemble the peri-nuclear structures in GOPC deficient spermatids as found in round-headed spermatozoa. *Arch Histol Cytol* 2004; **67**:349–360.
66. Kierszenbaum AL, Rivkin E, Tres LL, Yoder BK, Haycraft CJ, Bornens M, Rios RM. GMAP210 and IFT88 are present in the spermatid golgi apparatus and participate in the development of the acrosome-acroplaxome complex, head-tail coupling apparatus and tail. *Dev Dyn* 2011; **240**:723–736.
67. Nayernia K, Vauti F, Meinhardt A, Cadenas C, Schweyer S, Meyer BI, Schwandt I, Chowdhury K, Engel W, Arnold HH. Inactivation of a testis-specific Lis1 transcript in mice prevents spermatid differentiation and causes male infertility. *J Biol Chem* 2003; **278**: 48377–48385.
68. Kierszenbaum AL, Tres LL, Rivkin E, Kang-Decker N, van Deursen JMA. The acroplaxome is the docking site of Golgi-derived myosin Va/Rab27a/b- containing proacrosomal vesicles in wild-type and Hrb mutant mouse spermatids. *Biol Reprod* 2004; **70**:1400–1410.
69. Yildiz Y, Matern H, Thompson B, Allegood JC, Warren RL, Ramirez DMO, Hammer RE, Hamra FK, Matern S, Russell DW. Mutation of beta-glucosidase 2 causes glycolipid storage disease and impaired male fertility. *J Clin Invest* 2006; **116**:2985–2994.
70. Paiardi C, Pasini ME, Gioria M, Berruti G. Failure of acrosome formation and globozoospermia in the wobbler mouse, a Vps54 spontaneous recessive mutant. *Spermatogenesis* 2011; **1**:52–62.
71. Yuan S, Stratton CJ, Bao J, Zheng H, Bhetwal BP, Yanagimachi R, Yan W. Spata6 is required for normal assembly of the sperm connecting piece and tight head-tail conjunction. *Proc Natl Acad Sci USA* 2015; **112**:E430–E439.
72. Paranko J, Yagi A, Kuusisto M. Immunocytochemical detection of actin and 53 kDa polypeptide in the epididymal spermatozoa of rat and mouse. *Anat Rec* 1994; **240**:516–527.
73. Fouquet JP, Kann ML. Species-specific localization of actin in mammalian spermatozoa: fact or artifact? *Microsc Res Tech* 1992; **20**:251–258.
74. Howes EA, Hurst SM, Jones R. Actin and actin-binding proteins in bovine spermatozoa: potential role in membrane remodeling and intracellular signaling during epididymal maturation and the acrosome reaction. *J Androl* 2001; **22**:62–72.
75. Jeulin C, Lewin LM, Chevrier C, Schoevaert-Brossault D. Changes in flagellar movement of rat spermatozoa along the length of the epididymis: manual and computer-aided image analysis. *Cell Motil Cytoskeleton* 1996; **35**:147–161.
76. Miyata H, Satouh Y, Mashiko D, Muto M, Nozawa K, Shiba K, Fujihara Y, Isotani A, Inaba K, Ikawa M. Sperm calcineurin inhibition prevents mouse fertility with implications for male contraceptive. *Science* 2015; **350**:442–445.
77. Woolley DM, Neesen J, Vernon GG. Further studies on knockout mice lacking a functional dynein heavy chain (MDHC7). 2. A developmental explanation for the asthenozoospermia. *Cell Motil Cytoskeleton* 2005; **61**:74–82.
78. Bird Z, Hard R, Kanous KS, Lindemann CB. Interdoublet sliding in bovine spermatozoa: its relationship to flagellar motility and the action of inhibitory agents. *J Struct Biol* 1996; **116**: 418–428.
79. Kanous KS, Casey C, Lindemann CB. Inhibition of microtubule sliding by Ni2+ and Cd2+: evidence for a differential response of certain microtubule pairs within the bovine sperm axoneme. *Cell Motil Cytoskeleton* 1993; **26**:66–76.
80. Lesich KA, Zhang Z, Kelsch CB, Ponichter KL, Strauss JF III, Lindemann CB. Functional deficiencies and a reduced response to calcium in the flagellum of mouse sperm lacking SPAG16L. *Biol Reprod* 2010; **82**:736–744.
81. Lindemann CB, Fentie I, Rikmenspoel R. A selective effect of Ni2+ on wave initiation in bull sperm flagella. *J Cell Biol* 1980; **87**: 420–426.
82. Lindemann CB, Gibbons IR. Adenosine triphosphate-induced motility and sliding of filaments in mammalian sperm extracted with triton X-100. *J Cell Biol* 1975; **65**:147–162.
83. Lindemann CB, Orlando A, Kanous KS. The flagellar beat of rat sperm is organized by the interaction of two functionally distinct populations of dynein bridges with a stable central axonemal partition. *J Cell Sci* 1992; **102**:249–260.
84. Olson GE, Linck RW. Observations of the structural components of flagellar axonemes and central pair microtubules from rat sperm. *J Ultrastruct Res* 1977; **61**:21–43.
85. Woolley DM, Fawcett DW. The degeneration and disappearance of the centrioles during the development of the rat spermatozoon. *Anat Rec* 1973; **177**:289–301.
86. Avidor-Reiss T. Rapid evolution of sperm produces diverse centriole structures that reveal the most rudimentary structure needed for function. *Cell* 2018; **7**:n.pg.
87. Fishman EL, Jo K, Nguyen QPH, Kong D, Royfman R, Cekic AR, Khanal S, Miller AL, Simerly C, Schatten G, Loncarek J, Mennella V *et al.* A novel atypical sperm centriole is functional during human fertilization. *Nat Commun* 2018; **9**:2210.
88. Fawcett DW, Phillips DM. The fine structure and development of the neck region of the mammalian spermatozoon. *Anat Rec* 1969; **165**:153–183.
89. Ounjai P, Kim KD, Lishko PV, Downing KH. Three-dimensional structure of the bovine sperm connecting piece revealed by electron cryotomography. *Biol Reprod* 2012; **87**:73.
90. Woolley DM, Carter DA, Tilly GN. Compliance in the neck structures of the Guinea pig spermatozoon, as indicated by rapid freezing and electron microscopy. *J Anat* 2008; **213**: 336–341.

91. Kim J, Kwon JT, Jeong J, Kim J, Hong SH, Kim J, Park ZY, Chung KH, Eddy EM, Cho C. SPATC1L maintains the integrity of the sperm head-tail junction. *EMBO Rep* 2018; **19**: E45991.
92. Schoenenberger CA, Bischler N, Fahrenkrog B, Aebi U. Actin's propensity for dynamic filament patterning. *FEBS Lett* 2002; **529**: 27–33.
93. Fouquet J, Kann M, Soues S, Melki R. ARP1 in Golgi organisation and attachment of manchette microtubules to the nucleus during mammalian spermatogenesis. *J Cell Sci* 2000; **113**: 877–886.
94. Brahma S, Ngubo M, Paul S, Udugama M, Bartholomew B. The Arp8 and Arp4 module acts as a DNA sensor controlling INO80 chromatin remodeling. *Nat Commun* 2018; **9**:3309.
95. Peterson CL, Zhao Y, Chait BT. Subunits of the yeast SWI/SNF complex are members of the actin-related protein (ARP) family. *J Biol Chem* 1998; **273**:23641–23644.
96. Cairns BR, Erdjument-Bromage H, Tempst P, Winston F, Kornberg RD. Two actin-related proteins are shared functional components of the chromatin-remodeling complexes RSC and SWI/SNF. *Mol Cell* 1998; **2**:639–651.
97. Storey AJ, Wang HP, Protacio RU, Davidson MK, Tackett AJ, Wahls WP. Chromatin-mediated regulators of meiotic recombination revealed by proteomics of a recombination hotspot. *Epigenetics Chromatin* 2018; **11**:64.
98. Crapster JA, Rack PG, Hellmann ZJ, le AD, Adams CM, Leib RD, Elias JE, Perrino J, Behr B, Li Y, Lin J, Zeng H *et al.* HIPK4 is essential for murine spermiogenesis. *eLife* 2020; **9**:E50209.